Article:

Yu, R, Evans, AJ orcid.org/0000-0002-3524-1571 and Malleson, N orcid.org/0000-0002-6977-0615 (2018) Quantifying grazing patterns using a new growth function based on MODIS Leaf Area Index. Remote Sensing of Environment, 209. pp. 181-194. ISSN 0034-4257

https://doi.org/10.1016/j.rse.2018.02.034

Quantifying grazing patterns using a new growth function based on MODIS Leaf Area Index

Rui Yu[a]*, A.J.Evans.[a], N.Malleson[a]

*Correspondence: gyry@leeds.ac.uk

[a] School of Geography, University of Leeds, Woodhouse Lane, LS2 9JT Leeds, UK

Abstract

Monitoring grazing activities on grassland is crucial for ensuring sustainable grassland development and for protecting it from grazing-led degradation. The Leaf Area Index (LAI), which measures leaf coverage over a surface area, is commonly used as a proxy for grassland condition. However, current studies focus on the year-round or seasonal aggregated LAI change rather than the change that can be attributed explicitly to grazing, which is the important indicator for quantifying grassland grazing. This paper presents a new exponential growth function under grazing with an estimation algorithm, the purpose of which is to extract grazing-led LAI changes for every 8 days' satellite observations. All the analyses are based on the Moderate Resolution Imaging Spectroradiometer (MODIS) MOD15A2H products. An improved MODIS LAI and an expected LAI are produced separately, considering both current and previous grazing-led LAI changes. The differences between expected LAI and improved LAI are then converted to the equivalent carbon mass of grazed material. This grazed carbon mass is then aggregated within the growing season, and compared with the expected carbon mass consumed by livestock (calculated from statistics yearbooks). In addition, Net Primary Productivity (NPP) is produced using the improved LAI, simulated by a Light Use Efficiency with Vegetation Photosynthesis Model (LUE-VPM). This is compared with the NPP produced by LUE-VPM based on original MODIS LAI, MODIS NPP products (MOD17A2H) and grassland monitoring stations' in situ measured data. Results show that the NPP calculated from the improved LAI is statistically the same as in situ converted NPP with a p-value equalling 0.998 (the RMSE between the two is 97.77 gC/m2). Conversely, the p-value between converted in situ measured carbon mass and the MODIS NPP product is 0.011 (the RMSE between the two is 133.98 gC/m2), indicating they are statistically different. The results detailed in this paper provide precise and almost real-time grassland grazing monitoring information for policy makers managing grassland.

Keywords

Leaf Area Index (LAI)

MODIS

Grassland productivity

Livestock grazing

Light Use Efficiency (LUE)

1. Introduction

The Leaf Area Index (LAI) is generally defined as the total one-sided green leaf area per unit ground area for flat broadleaf plants (Monteith and Reifsnyder 1974) or one-half the total green leaf area per unit ground area for needles of conifers (Chen and Black 1992). It is a dimensionless value, and descriptive statistics such as the range or the aggregated LAI are directly comparable over time and sites as the resulting numbers are absolute values (Asam et al. 2015). The LAI is a key parameter for assessing the carbon and energy in the biosphere (Swain et al. 2016; Verger et al. 2015; Zhang et al. 2016), photosynthesis (Verrelst et al. 2016; Wei et al. 2016) and biomass production (Prieto-Blanco et al. 2009). Empirically, the amount of total solar radiation intercepted by a canopy is often well correlated with the production of dry matter during periods when the leaf area index is increasing (Russell et al. 1990); and extending from this observation, numerous vegetation Net Primary Productivity

(NPP) models use LAI as a key proxy of canopy status in quantifying the solar radiation interception (Ruimy et al. 1999).

The in-situ LAI of plant canopies can be obtained either directly by green leaf collection or indirectly by examining the physical properties of green leaves; a detailed discussion on these measurements was presented in Jonckheere et al. (2004). Large-scale in-situ measurement of LAI is almost impossible due to its labour-intensive character (Jonckheere et al. 2004). Remote sensing of vegetation spectral information acquired from moderate resolution optical sensors provides an alternative means of observing canopy LAI, which largely extended the LAI observation from regional to global (Buermann et al. 2001; Tian et al. 2004). Datasets such as the 10 day CYCLOPES LAI (Baret et al. 2007), which uses neural networks over a radiative transfer model (Verhoef 1984) at about 1km spatial resolution from 1998 to 2003; and GLOBCARBON (Deng et al. 2006) from Satellites Pour l'Observation de (SPOT/VEGETATION) from 1997 to 2003, which is calculated through a Four-Scale bidirectional reflectance model (Chen and Leblanc 1997) at about 1 km resolution; or Moderate Resolution Imaging Spectroradiometer LAI (MODIS LAI, which is based on a 3D radiative transfer model (Knyazikhin et al. 1998a) with about 0.5 km resolution) from TERRA-AQUA sensors since 2000 (Yang et al. 2006) report the global vegetation LAI. We use MODIS LAI for its high spatial resolution and data availability during 2003~2012.

The LAI datasets derived from remote sensing are extensively employed in the field of grassland monitoring (Field et al. 1995; Gao et al. 2013; Piñeiro et al. 2006; Potter et al. 1993). Among them, the MODIS LAI dataset is one of the most widely used (Fang et al. 2008; Hill et al. 2006). MODIS LAI reduces the effects of soil conditions (Fang et al. 2015), local viewing and illumination conditions (Croft et al. 2014; Galvão et al. 2013; Los et al. 2005) and canopy structure (Croft et al. 2014), by taking the canopy and scene geometry specifications into account during estimation (Jensen et al. 2011). Therefore, MODIS LAI changes, especially time-series changes, are suitable and consistent for the detection of vegetation status changes. MODIS LAI are widely used and extensively validated around the world (De Kauwe et al. 2011). For example: by comparing the LAI of two different catchments in South Africa, Palmer and Bennett (2013) use MODIS LAI to identify the grassland degradation of communal grasslands. Similarly, Bobée et al. (2012b) reported the seasonal dynamics of grasslands by the employment of time series MODIS LAI observations. Mayr and Samimi (2015) further validated the consistency of MODIS LAI by comparing the spatial patterns of field-measured LAI, LAI derived from High-Resolution RapidEye Imagery and MODIS LAI.

MODIS LAI retrieval techniques are mainly based on the spectral and angular samplings of the radiation field reflected by vegetation canopies. The MODIS LAI algorithm uses a main Look-up-Table to retrieve LAI values (Wang et al. 2004). A three-dimensional radiative transfer equation is used to derive spectral and angular biome-specific reflectances of vegetation canopies (Knyazikhin et al. 1998a). The numerical solutions of this equation are calculated and stored in the Look-up-Table. It provides the best fit LAI to measured data by considering background effects (soil reflection), and biome-specific spectral and angular information for vegetation (Knyazikhin et al. 1998b). But in some instances, the algorithm may fail and an empirical LAI would generally be used to fill pixels where this is the case. For example; radiation is strongly affected by clouds, meaning that the MODIS LAI needs to be reprocessed before use. Current reprocessing methods are focused on producing a smoother and more spatiotemporally consistent product by taking a spatial, temporal or hybrid combination of weighted LAI values into account (Fang et al. 2008; Hansen et al. 2003; Liu et al. 2017; Xiao et al. 2011; Yuan et al. 2011; Zhang et al. 2012). These improved LAI estimates are widely used for a broad view of pixel-specific vegetation dynamics at both regional scale (Bobée et al. 2012a; Jin et al. 2017) and global scale (Zhang et al. 2017).

However, when looking into the vegetation dynamics for each time period in grazing monitoring, the improved LAI dataset has the disadvantage that it demolishes the original grazing information through spatiotemporal averaging. In the context of grassland, especially in grazing intense areas (Gignoux et al. 2001), the grazing-led LAI changes caused by livestock grazing could have a significant effect on the quantity and quality of grass productivity (Matches 1992). Remote sensing data can only capture the time period status of vegetation, rather than the whole process of vegetation development; nevertheless, improvements can be made. Ignorance of the grazing activities that may cause LAI change can lead to underestimates or otherwise incorrect assessments of grassland productivity, especially in grazing intensive regions (Lebert et al. 2006; Nyima 2015). This is important for grassland management, and researchers have argued that grazing coupled with climate change are the main factors contributing to regional grassland degradation and even desertification (Dean et al. 1995; Harris 2010). It may directly lead to the change from green land to bare land, and a grazing-led LAI change could be observed in the grass growth season (Miller-Goodman et al. 1999; Tsalyuk et al. 2015).

It is of great importance to identify the spatial distribution and quantity of grazing-led LAI changes on grasslands. The aim of this paper is therefore to estimate these changes using MODIS LAI datasets. However, the information we have from MODIS LAI datasets is very limited with regards to extracting the precise changes directly. Therefore, we need to further process the available datasets. The accurate quantification of grazing-led LAI changes would produce a crucial indicator that would be used to guide sustainable grazing pasture management.

There are two main difficulties directly or indirectly related to the MODIS LAI datasets:

- MODIS LAI datasets are inevitably affected by clouds or other modelling errors (Myneni et al. 2015). When we only use “good quality” data, the other pixels (non-good quality) make the dataset discontinuous. We need to pre-emptively decide how to fill these "non-good quality" pixels reasonably and consistently in a manner that is best for estimating grazing-led LAI changes on grassland.

- The question of how to estimate the grazing-led LAI changes during the grass growing season is based on the LAI after grazing observed by MODIS. This depends on how we calculate the expected LAI before grazing. For a specified pixel, both the effect of current grazing and previous grazing should be considered simultaneously.

To solve these two problems, we need to develop a new integrated growth grazing function that is able to describe seasonal growth cycles of the grass under grazing. It can be used to fill these "non-good quality" pixels more reasonable according to grass phenological dynamics. The grazing-led LAI changes can then be derived by fitting to this new growth function. Since there are no direct data to validate the estimation of grazing-led LAI changes, we use two indirect measures to validate it: the expected carbon mass consumed by livestock and the land Net Primary Productivity (NPP).

2. Data sources

The case study area for this work is Zeku County, Qinghai, China. The total land area is approximately 6600 km^2, of which grassland accounts for 98%. The elevation is above 3500 meters for the vast majority of the land, with the highest elevation being 4971 meters and the lowest being 2800 meters. The year-round mean temperature ranges from -3 ℃ to 2.8 ℃ (the average annual temperature is -1.1℃ with a deviation of 0.84 ℃), with no absolute frost-free period.

2.1. Household survey data

The household data used in this study originate mainly from a field survey conducted in 2012 by the Centre for Chinese Agricultural Policy (Huang et al. 2016). This field survey was supported by the National Key Programme for Developing Basic Science (2012CB95570001) project "Impact of Climate Change on Key Parameters of Socio-economic System in Typical Regions", which was led by the Centre for Chinese Agricultural Policy, Chinese Academy of Science. The first author was part of the survey team. Zeku was one of the three selected typical counties in the survey. The towns and villages within Zeku were randomly chosen for inclusion, and the sampling size was 52 households. The sampling data include the number of livestock, the winter/summer pasture area and the land tenure for each household. The percentage of winter pasture area is 44.8% for Zeku in 2011 according to the survey. This percentage is mainly used to filter out the small LAI changes in un-grazed pixels, that is, the percentage of winter pasture area derived from MODIS LAI should be the same as that of household survey statistics. Although the survey size is relatively small, its results are useful because it gives the information of the grazing land (percentage of winter/summer pasture area), and represents characteristic of the grassland grazing in the local area (Huang et al. 2017).

The survey also showed that there are herbivores other than agricultural livestock present in the area, and, indeed, that some species (such as Stipa purpurea) are even threatening the stability of the rangeland ecosystem in places. However, this paper does not consider the effect of other herbivores due to the fact that the livestock grazing has a dominant role in the rangeland forage consumption.

2.2. Image datasets

Two image datasets were employed to assess the Leaf Area Index (LAI). These are MODIS LAI and GlobalLand30 land use/cover datasets. GlobalLand30 land use/cover datasets were used to extract the spatial distribution of grassland in Zeku. The MODIS LAI datasets were used to estimate the LAI value of grassland. Both datasets were projected to Krasovsky 1940 Albers, with central meridian 105°, standard parallel 25° and 47°. The projection kept the projected land area the same as that of the earth's surface, which is important for the validation of grazing-led LAI changes.

2.21. MODIS LAI products (MOD15A2H006)

The LAI datasets were gathered from the MODIS collection 6 LAI (MOD15A2H006) (Myneni and K. 2015). For each pixel (approximately 463 m×463 m) during 2003-2012, the data contain a LAI estimate as well as an 8-bit quality control (QC) value (Myneni et al. 2015). The LAI is unitless (m^2/m^2) and the scale factor is 0.1 (meaning the real value is 10 times smaller than that of the MODIS LAI).

In this paper, only the "good quality" data with QC=0 were used in order to avoid introducing any further uncertainties into the model. In the MODIS LAI dataset, there are LAI observations every 8 days which in total is 46 observations each year. These are the "best" pixels available from all the acquisitions of the Terra sensor from within the 8- day period. The time range of the dataset is from 2003 to 2012. The average percentage of the number of "good quality" (QC=0) pixels to the total number of grassland pixels is shown in Fig. 1, the average ratio is 81.52% for Zeku during 2003~2012.

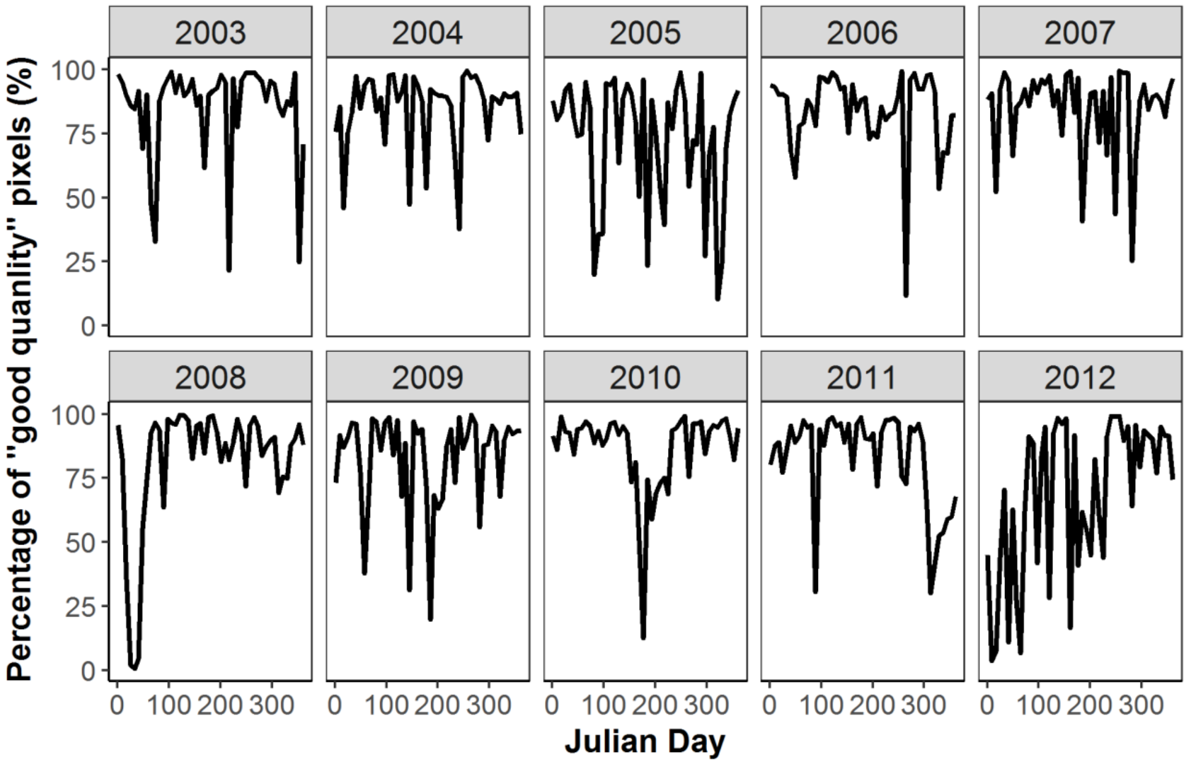

Fig. 1: Percentage of “good quality” (QC=0) pixels for MODIS LAI in Zeku, China

2.22. GlobalLand30 datasets

The land cover data, used in this study to identify grasslands were from the 30 meter Global Land Cover dataset (GlobalLand30). The overall classification accuracy reached 83.51% (Kappa= 0.78). Specifically, the accuracy for grassland was 76.88% (Chen et al. 2015). As it was organized into tiles, four tiles were downloaded to cover the extent of Zeku County (tile numbers are: N47_30_2010LC030, N47_35_2010LC030, N48_30_2010LC030, and N48_35_2010LC030). After mosaicing, re-projection and extraction, the data were resampled to approximately 463×463m^2 spatial resolution (this is the same pixel size as in the MOD15A2H006 LAI datasets) by the majority percentage principle. The land cover in the year 2010 is shown in Fig. 2. Because there are almost no changes in land cover when compared with the data in 2000, it is assumed that Land Cover type has not been changed substantially during the modelling period (2003~2012).

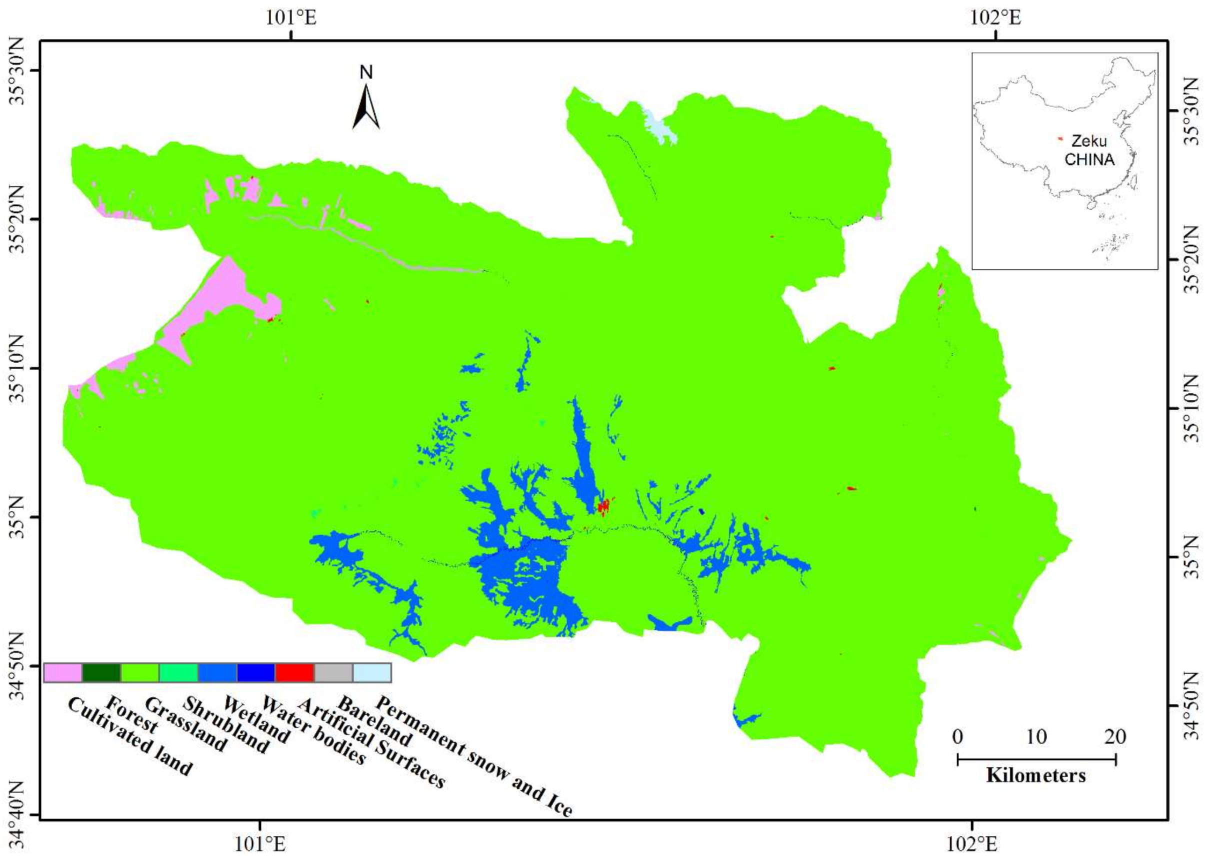

Fig. 2: Land Cover of Zeku, 2010

2.3. Validation datasets

In order to validate the new LAI estimation (that takes account of grassland grazing), two types of datasets were used.

2.3.1 Net Primary Productivity Validation

The first data set was related to the improved LAI validation, which involves the calculation of Net Primary Productivity (NPP) from the LAI and a comparison with some in-situ grass fresh weight data, provided by The Grassland and Livestock Husbandry Bureau of Zeku that was collected in 2016. There were 15 grassland sampling sites and 4 samples were taken for each site, and the size was 1 m^2 for each sample. These are the Chinese national grassland monitoring sites, which were chosen depending on the representativeness of the overall grass growth. We used the average fresh weight for each sampling site. Two datasets are used in the NPP calculation. Both datasets are projected to Krasovsky 1940 Albers. The first is daily temperature data, which are downloaded from the High-Resolution China Meteorological Forcing Dataset (0.1° spatial resolution for every 3 hours from 2003 to 2012) (He and Yang 2011). The daily average temperature is calculated and resampled (using mean value for the mixed pixel) to the same spatial resolution as MODIS LAI.

The second NPP-validation data includes the daily surface reflectance and is available online from MODIS MOD09A1 surface reflectance datasets (Vermote 2015) from 2003 to 2012. These data have the same spatial resolution as MODIS LAI (about $463 \times 463 m^2$). The temporal resolution is 8-day periods. For each day in the 8-day period, the surface reflectance is calculated through the weighted average of its former surface reflectance and current reflectance; they are linearly interpolated to daily surface reflectance data for daily NPP calculation.

2.3.2 Livestock Validation

The second validation dataset is related to the validation of grazing-led LAI changes. This includes the number of livestock (yak, sheep, goat, and horse) during the grass growth period, which has been provided by the Statistical Bureau of Zeku from 2003 to 2012. The Statistical Bureau of Zeku collects the number of livestock for the whole county every year through a household survey at each village.

3. Methods

The estimation of grazing-led LAI changes is mainly based on the analysis of MODIS LAI datasets. The framework is shown in Fig. 3:

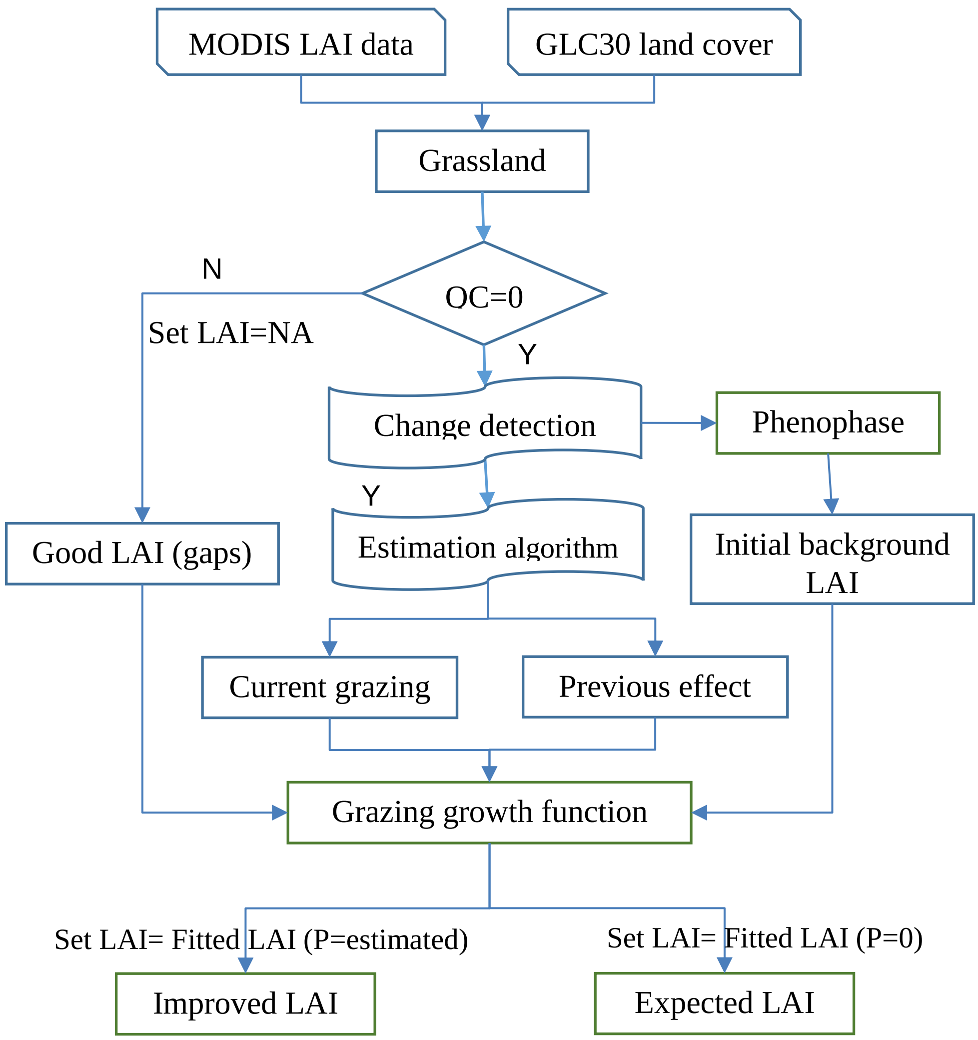

Fig. 3: Conceptual framework for quantifying grazing based on LAI data

After extracting the grassland LAI of Zeku based on MODIS LAI and GLO30 land use/cover datasets from 2003 to 2012, the “good quality” LAI data were retained by setting the LAI value of “non-good quality” pixels to “NA”. The retained “good quality” LAI data are not continuous over 46 observations during the year due to the “NA” settings. We use the new growth function to calculate the value of these “NA” pixels.

In this paper, we focus only on the grass growth period for the estimation of grazing-led LAI changes. This is because the LAI is largely static during the winter period for grassland in Zeku. MODIS LAI can capture limited grass information in winter due to the grassland burning in Zeku, such that the LAI values mainly report the background soil information. In order to distinguish the grass growth period and non-growth periods, which will be used to calculate initial background LAI, the first work in this paper is to detect the phenophase of the grassland. A change detection technique was employed to estimate the starting date and end date of the grass growing season. The initial background LAI (mainly soil information) can be calculated after phenophase detection.

A new grass growth function will be developed to describe grass growth under grazing. In order to fit this new growth function, the initial background LAI, current LAI (MODIS “good quality” LAI) and the expected LAI (LAI before grazing with the effect of the previous grazing) should be known. An estimation algorithm is then developed to extract the value of the expected LAI for each pixel, which considers both current grazing and the effect of the previous grazing. Finally, by curve fitting, an improved LAI and expected LAI will be produced. The grazing-led LAI change is then the difference between expected LAI and improved LAI. Next, this new growth function will be introduced.

3.1. New growth function

One way to estimate the grazing-led LAI change is to estimate the full growth curve and compare it with the recorded LAI for each pixel. There is a history of research devoted to finding a simple function that describes the basic LAI dynamics of grass. For perennial grasses, which are the dominant species in the Zeku, Qinghai-Tibet area, the LAI within the whole season can be described by three stages (Fig. 4). These stages can be observed both in field measurements (Hoffmann et al. 2005) and by remote sensing (Garrigues et al. 2008; Xiao et al. 2011). The LAI estimation process developed here starts by identifying the grazing-led LAI changes caused by livestock during the grass growing season for each 8-day period. The parameters of this new growth function for each pixel are estimated though fitting against the MODIS LAI dataset.

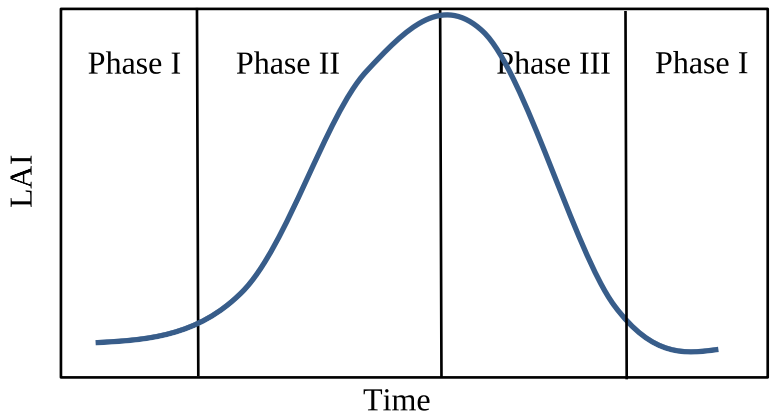

Fig. 4: LAI during a regrowth follows a bell curve as the canopy develops from low LAI (Phase I: low LAI increase rate) to maximum LAI (Phase II: high increase rate, growth dominated) and then to low LAI again (Phase 3: high LAI decrease, senescence dominated).

The ordinary exponential growth function as detailed in Johnson and Thornley (1983) and Thornley and Johnson (1990) is widely used, but there are two problems that need to be further considered when describing the LAI changes:

1. The senescence factor is totally ignored;
2. A lack of parameters that can represent the grazing effect.

A feasible way to deal with those problems is to add a senescence defoliation coefficient (the leaf changes colour from green to yellow) and grazing-led defoliation coefficient (the leaf is partly consumed by livestock) to the exponential growth function according to the nature of plant development. In this way, the whole processes of plant development (see Fig. 4) can be described appropriately in one function, while the traditional growth function can only describe growth dominated period (Phase I and Phase II in Fig. 4). When considering livestock grazing and grass senescence, the new function can be expressed as:

$$\frac{d(L_t+G_t+GB_t)}{dt} = k_1(L_t + G_t + GB_t) - k_2(L_t + G_t + GB_t)t$$

Where L_t is the current LAI that can be observed; G_t is the grazing-led LAI loss; and GB_t is the previous grazing effect on current LAI. $k_1(L_t + G_t + GB_t)$ represents the current total growth rate, which is proportional to the current LAI. This has been widely examined in ecological related studies (Johnson and Thornley 1983; Thornley and Johnson 1990).

$k_2(L_t + G_t + GB_t)t$ represents the total senescence rate, and is proportional to the current LAI. Notice that it takes the time as a weight; $\mathrm{f}(t) = t$, and is calculated in a time-dependent manner. According to the observations from Borrás et al. (2003) and Leopold et al. (1959), the total senescence rate is linear to time t. Although this relationship may be linear or non-linear across plant species, this paper assumes a linear relationship for simplicity. There is an improvement that can be made to the function; given the quantity of growth is the effect of growth and senescence combined, that growth is proportional to its current LAI (L_t). Equally, as the senescence rate can be related to both current LAI (L_t) and time t, it can be written as:

$$\frac{d(L_t+G_{t+GB_t})}{(L_t+G_t+GB_t)} = (k_1 - k_2 t)d_t$$

Then to integrate this equation:

$$\int_{L_0}^{L_t} \frac{d(L_t+G_{t+}+GB_t)}{(L_t+G_t+GB_t)} = \int_0^t (k_1 - k_2 t)d_t$$

where $\mathrm{L}(\mathrm{t} = 0) = L_0$ is the initial background LAI. This equation is now can be solved to have:

$$ln\frac{(L_t+G_t+GB_t)}{(L_0+G_0+GB_0)} = k_1 t - k_2 t^2 + C.$$

In fact, at the start, $G_0 = GB_0 = 0$; C is the constant after integration, and therefore we have:

$$\frac{L_t+G_t+GB_t}{L_0+G_0+GB_0} = \frac{L_t+G_t+GB_t}{L_0} = \frac{L_t+G_t+GB_t}{L_t} * \frac{L_t}{L_0} = \frac{1}{P} * \frac{L_t}{L_0} = \frac{L_t}{PL_0}$$

where P is defined as the percentage of LAI which has been observed (remaining LAI after grazing):

$$P_t = \frac{L_t}{L_t+G_t+GB_t}.$$

If we substitute this to the integrated growth equation, we get:

$$L_t = L_0 P e^{k_1 t - k_2 t^2 + C} \ ,$$

which is the basic form of the new growth model. When using this model, an initial background LAI value (L_m, or background value) is set, as this is more convenient when fitting the observed data. In fact $L_t = L_{observed} - L_m$, thus, it becomes:

$$L_{observed} = L_m + L_0 P_t e^{k_1 t - k_2 t^2 + C}$$

and usually, $L_m = L_0 = \min\{L_t\}$.

We additionally define

$$PB_t = \frac{GB_t}{L_t + G_t + GB_t}$$

$$PG_t = \frac{G_t}{L_t + G_t + GB_t}$$

where PG_t is the percentage of current grazing-led LAI change and PB_t is the effect of previous grazing on LAI change. Then we can have the following relation between PB_t, PG_t and P_t:

$$P_t = 1 - PB_t - PG_t \quad .$$

Substitute this to $L_{observed} = L_m + L_0 P_t e^{k_1 t - k_2 t^2 + C}$ and we have the final equation:

$$L_{observed} = L_m + L_0 (1 - PB_t - PG_t) e^{k_1 t - k_2 t^2 + C}$$

In general, this new growth-grazing function can improve the accuracy of the regression coefficient if we intend to find a curve across the sample points that match as reasonably as possible. However, this new growth-grazing function is not enough in isolation; it needs to be accompanied by a grazed LAI estimation algorithm where PB_t and P_t will be estimated, as discussed in Section 2.3.4.

In the next section, we will outline the components of a curve fitting procedure with regard to this new growth function. This procedure follows the framework outlined in Fig. 3.

3.2. Step 1: phenophase detection

The first element of the analysis is identifying the grass growth period. To do this, we utilise change point detection, applied to the 8-day MODIS LAI data time series. The purpose of the change point detection is to identify the location of change (single or multiple) in the statistical properties of a sequence of observations that change in the series data. The cost-penalty function is a commonly used method (Killick and Eckley 2014) to measure such change locations that minimize:

$$\sum_{i=1}^{m+1}\left(\rho y_{(\tau_{i-1}+1)}:\tau_i\right)+\beta f(m)$$

where ρ is a cost function for a segment, the log-likelihood is a commonly used cost function (Horváth 1993); τ_i is the ith change point and the total number of change points is m; $y_{(\tau_{i-1}+1)}:\tau_i$ represent the ith segment, the $\beta f(m)$ is a penalty to guard against over fitting. We use the PELT method, which assumes that the penalty is linear to the number of change points, that is, $\beta f(m) = \beta m$ (Jackson et al. 2005; Killick et al. 2012), as a choice of penalty function with Modified Bayes Information Criterion (Zhang and Siegmund 2007). For this research, we need to identify the change point where the mean value of the ith segment has a maximum likelihood statistic which minimizes the value of cost-penalty function. The change detection software used here is the R “changepoint” package developed by Killick and Eckley (2014). At least two change points would be expected according to Phase I in Fig. 4: the start and end date for grass growth.

3.3. Step 2: generating initial background LAI

After identifying the phenophase using a change point detection technique, the initial background LAI can be calculated using the LAI data during winter periods. There are various methods that can be used to calculate the initial background LAI. On the global scale, a series of calculation algorithms are integrated in the background LAI calculation schema (Yuan et al. 2011), which consists of a conditional multi-year average, TIMESAT (a software package to analyse time-series of satellite sensor data) Savitzky–Golay (SG) filter (Savitzky and Golay 1964), local per class mean (average LAI value with a small area for each land use/cover type), per class mean (average LAI value for each land use/cover type) and multi-year per class mean (multi-year average LAI value for each land use/cover type) (Yuan et al. 2011). In addition, improved ecosystem curve fitting (VCF-ECF) has been proved a useful method in producing continuous field products (Hansen et al. 2003). However, these methods are not applicable at Zeku, or, indeed, any other area where grazing is important in calculating carbon cycling. All of these methods are focused on producing smooth and consistent values of LAI, while in the grazing-intensified grassland areas in Zeku, any attempt to produce the average or weighted average of LAI, either spatially or temporally, would directly reduce or eliminate the effect of grazing. In addition, prescript grassland burning during winter is commonly seen in Zeku, which results in the same value of LAI during the winter period (determined by the results of phenophase detection). We, therefore, use the modal value of LAI during winter period from 2003 to 2012 as the initial background LAI.

3.4. Step 3: preliminary estimation for current grazing and the effect of the previous grazing

The next step is to estimate the grazing-led LAI changes for each pixel preliminarily. The value of this estimation will be improved by fitting with the new growth function. For each pixel, here we define the following:

- Full growth LAI is the theoretical LAI curve if there is no grazing (without the effect of previous grazing and current grazing);
- Expected LAI is the LAI before grazing (with effect of the previous grazing but without effect of current grazing);
- Observed LAI is the LAI after grazing (with the effect of current grazing and previous grazing).

The observed LAI is a time-series of point data. When there is an adverse observed LAI value, we can calculate the expected LAI and compare it to that of the observed LAI. The field measurement LAI of grazing treatment suggest that when grazing stops, grassland can regrow to pre-grazing levels (Harrison et al. 2012). Taking this model, we assume that local maxima in the growth curves represent expected seasonal growth for grazed pixels. An illustration of how the grazing-led LAI changes are calculated is shown in Fig. 7 and elucidated below:

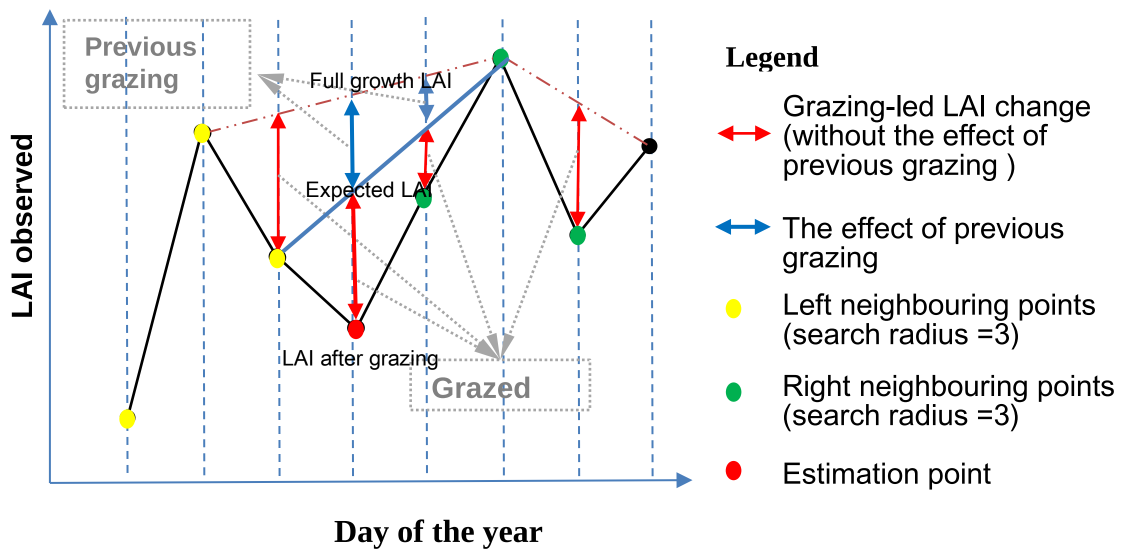

Fig. 5: Estimation of grazing-led LAI changes estimation

For example, the red point in the figure represents the current estimation point i, yellow points are the left neighbouring points with neighbourhood radius 3 (for MODIS, the unit is an 8-day period), while the green points are the right neighbours. The grazed LAI is then the difference between expected LAI and observed LAI (arrowed red segments). The effect of the previous grazing on current growth is calculated by the difference of full growth LAI and expected LAI (arrowed blue segments). The algorithm can be summarised as:

- for each time slice point i (the i^{th} observation recorded by MODIS LAI, i=1, 2…46), the time-series LAI point data are divided into its left neighbour points set (from point i-r to point i-1) and right neighbour points set (from point i+1 to point i+r) by a predefined neighbourhood radius r, r is the radii, ranging from 1 to 46, and is defined as the radii to search the neighbouring points for the current estimation point. The values of the radii range from 1 to 21 which is enough to estimate in all situations. The estimation algorithm chooses the radius which minimizes the average fitting residual for each pixel as the optimal neighbourhood radius for each pixel.

- Search for the point with maximum LAI in the left neighbouring points set and right neighbouring points set separately (the left maximum LAI point $P_m = \max(P_{i-r}, \dots, P_{i-1})$ and the right maximum LAI point $P_n = \max(P_{i+1}, \dots, P_{i+r})$).
- Calculate the full LAI for point i, utilising the time difference as a weight,
  - ✓ if $P_m < P_n$, the full LAI is: $LAI_{full} = P_m + \frac{i-m}{n-m} * (P_n - P_m)$
  - ✓ if $P_m > P_n$, the full LAI is: $LAI_{full} = P_n + \frac{n-i}{n-m} * (P_m - P_n)$
  - ✓ if $P_m = P_n$, the full LAI is: $LAI_{full} = P_m = P_n$
- Calculate the difference between full LAI and observed LAI. If this difference is bigger than zero, calculate the observed percentage of LAI by: $P_i = \frac{LAI_{P_i}}{LAI_{P_i} + difference}$; if not, this percentage will be set to 1.
- If the previously observed percentage of LAI P_{i-1} is smaller than 1, change the left neighbour to point i-1, do step 3 and we can get PB_i; If not, set $PB_i = 0$; PG_i can be calculated by $PG_t = 1 - PB_t - P_t$;
- The estimation error can be evaluated by using the sigma value of the nonlinear fitting of the new growth function, which indicates the average fitting residual.

Having preliminarily estimated the grazing-led LAI changes and full growth for each point on the per-pixel LAI curve, and knowing the initial background LAI, the analysis can proceed to fit the growth curve to the observed growth points, filling in the “non-good quality” pixels (improved LAI). The improved LAI can be calculated by the new growth equation directly; while the expected LAI is calculated by setting PG_t=0 (the percentage of current grazing). The expected LAI is calculated by making sure that the percentage of winter pasture area (44.8%) is the same as the percentage of the pixels that are estimated to have no grazing. We use the percentage of pixels to filter out the smallest estimated grazing-led LAI changes. The expected LAI is then calculated by setting the preliminary estimation of grazing-led LAI changes to 0 ($P_t = 1$, $PB_i =$ estimated PB_i and $PG_t = 0$). Note PB_t should stay the same, as has been calculated in step five. This is because whole estimation algorithm depends on the previous status of vegetation, and if there is no grazing at the current time period it does not mean the previous time period had no grazing as well. The grazing-led LAI change (without the effect of previous grazing) can then be calculated by taking the difference between expected LAI and improved LAI.

3.5. Step 4: validation of improved LAI

Before we validate the estimated grazing-led LAI changes in this paper, the improved LAI which was produced by the new exponential growth function should be validated first. There are no in-situ measured LAI data for Zeku with which we could validate the improved LAI. Instead, we compare the aboveground Net Primary Productivity (NPP) produced by the improved LAI with in-situ measured grass weight data that were collected from the Grassland Livestock Bureau of Zeku.

To calculate the NPP, based on the improved LAI, we here utilise the Light Use Efficiency with Vegetation Photosynthesis Model (LUE-VPM) which is widely used in NPP estimation, most specifically by MODIS, to produce their global 500m and 1000m NPP data. The difference between the LUE-VPM model in this paper and the conventional model used in the MODIS data is that the Vapour Pressure Deficit (VPD) attenuation scalar is replaced by a Vegetation Photosynthesis Model (VPM) scalar due to data limitations; for more information on the VPM construction, see (Xiao et al. 2004). The key parameters and datasets for the MODIS NPP calculation and LUE-VPM are shown in Table 1:

Table 1: model parameters of NPP calculation

	MODIS (Running and Zhao 2015)	LUE-VPM (Light Use Efficiency with Vegetation Photosynthesis Model)
Light Use efficiency (LUE)	Vapour Pressure Deficit (VPD)	Vegetation Photosynthesis Model (VPM) (Xiao et al. 2004)
Maximum radiation conversion efficiency (ε_{max}, KgC/m^2 /d/MJ)	0.00086	0.00061(Li et al. 2012)
Photosynthetic Active Radiation (PAR) data	from Global Modelling and Assimilation Office (GMAO/NASA)	calculated by Area Solar Radiation (Fu and Rich 2002)
The fraction of Photosynthetically Active Radiation absorbed by vegetation (fPAR) data	from MODIS fPAR	calculated with Beer-Lambert law (Ruimy et al. 1999)

Another work is to convert grass fresh weight (g/m^2) to NPP (gC/m^2). The relation between aboveground dry matter (ADM) and NPP can be described as (Maselli et al. 2013; Running 2015):

$$\mathrm{NPP} = \mathrm{ADM} * (Root\_Leaf\_Ratio + 1) * 0.5$$

where the multiplier $(Root\_Leaf\_Ratio + 1)$ converts the above ground dry matter to whole plant dry matter (both above ground mass and below ground mass). This value is taken as 0.28 following Running (2015). The 0.5 multiplier accounts for the conversion from dry matter to carbon (Maselli et al. 2013). The ratio of ADM to above ground fresh grass weight in Zeku is 0.37 according to Lai et al. (2008).

3.6. Step 5: validation of grazing-led LAI changes

The LAI should decrease in proportion to the amount eaten during grazing (Johnson et al. 2010). One direct way to validate the accuracy of grazed LAI estimation is to measure LAI at both pre-grazing and post-grazing sites for every 8 days during the growth period. However, this would require continuous sampling on the same site for years. An alternative method is to compare the grazed LAI estimate with the total carbon mass consumption of the livestock during grass growth period for each year. To calculate the livestock consumption, all the livestock including sheep, goat, yak and horse are converted to Sheep Units (SU), then according to the SU conversion coefficient (Table 2, see NY/T635 (2002)), the carbon consumption is calculated during the grazing period for each year using the follow formula:

$$\begin{aligned}\text{Raised Sheep Unit} &= \left(livestock_{total_{start}} - livestock_{young_{start}}\right) * SUcoe_{mature} \\ &+ \left(livestock_{young_{start}} + livestock_{young_{increase}}\right) * SUcoe_{young} \\ &- \left(livestock_{total_{dead}} - livestock_{young_{dead}}\right) * SUcoe_{mature} * Coef_{die} \\ &- livestock_{young_{dead}} * SUcoe_{young} * Coef_{die}\end{aligned}$$

$$\text{Carbon Mass} = \text{Raised Sheep Unit} * \text{GrassDryWeight}_{perSU}/0.5 * 155$$

For each livestock type (sheep, goat, yak, and horse), $livestock_{total_{start}}$ is the total number of livestock at the start of the year; $livestock_{young_{start}}$ is the number of young livestock at the start of the year; $livestock_{young_{increase}}$ is the number of livestock increased during the year; $livestock_{total_{dead}}$ and $livestock_{young_{dead}}$ is the number of total and young dead livestock respectively during the year; $SUcoe_{mature}$ and $SUcoe_{young}$ is the SU convert coefficient for mature and young livestock (Table 2); $Coef_{die}$ is the percentage of livestock dead before grazing period (here we give this a constant value 0.5, assuming the number of dead livestock is evenly distributed during the year). In Zeku, the herders treasure livestock as an embodied fortune, and the livestock are mainly sold after the grass growth period according to our field survey. After calculating SU, the SU is converted to carbon mass using the second equation. The 0.5 multiplier accounts for the conversion from dry matter to carbon (Maselli et al., 2013), and 155 is the total grazing days during the grass growth period according to Fan et al. (2010b). $\mathrm{GrassDryWeight}_{perSU}$ is the dry grass consumed per SU, the value is 1.8 kg day^{-1} according to (Fan et al. 2010a).

Table 2: livestock conversion coefficients:

Livestock Type	Mature (sheep unit)	Young (sheep unit)
Sheep	1	0.4*1
Goat	0.8	0.4*1
Yak	4.5	0.3*4.5
Horse	6.0	0.3*6.0

To compare with the estimated carbon mass, the grazing-led LAI changes (without the effect of the previous grazing) are converted to carbon mass according to Johnson et al. (2010):

$$\mathrm{LeafMass} = \mathrm{LAI}/\sigma$$

where σ is the Specific Leaf Area, we take the same value in the MODIS Biome-Property Look Up Table (Running et al. 2000).

4 Results

3.1. Grass growth under different defoliation severity estimates

The indicator used in this paper is the Leaf Area Index (LAI), which will be used to extract grazing information according to time series change following the methodology above. Here, the example theoretical results generated by the new growth function under three different grazing defoliation severities are shown in Fig. 6. The results show that different grazing regimes do have a significant effect on observed LAI. A larger percentage of grazed LAI means there will be a smaller observed LAI. The same is true for the instantaneous growth rate of LAI.

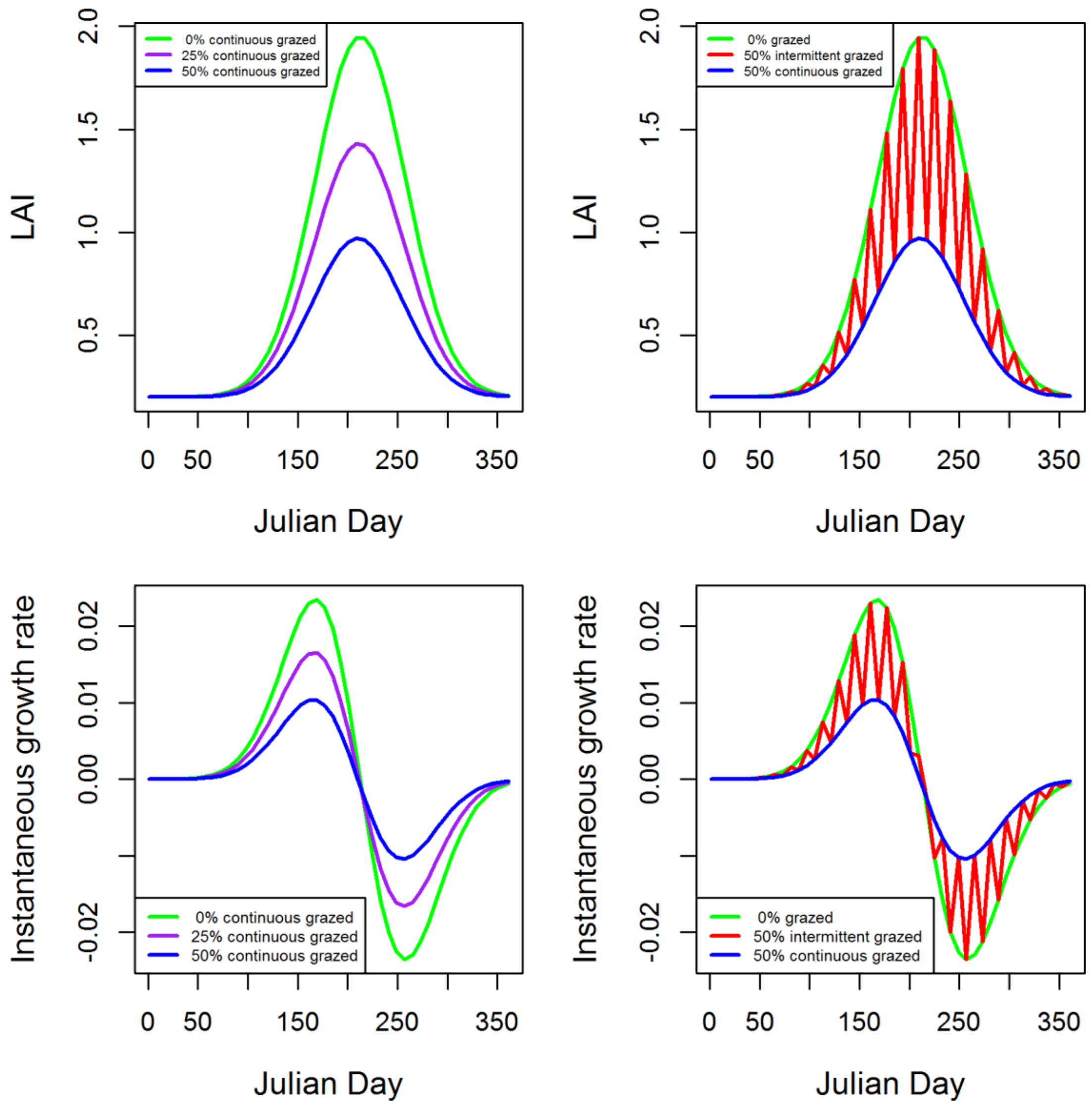

Fig. 6: The effect of grazing severity on the observed LAI and instantaneous net growth rate of LAI, with for example k1= 0.16, k2=0.0003, C=-14. c and d are $L_t{}'$

3.2. Results of phenophase by change point detection

Figure 7 shows the mean LAI distribution for all pixels from 2003 to 2014, from which the most conservative change points were chosen as the start and end dates of the growth season. There is a basic symmetrical trend for each year.

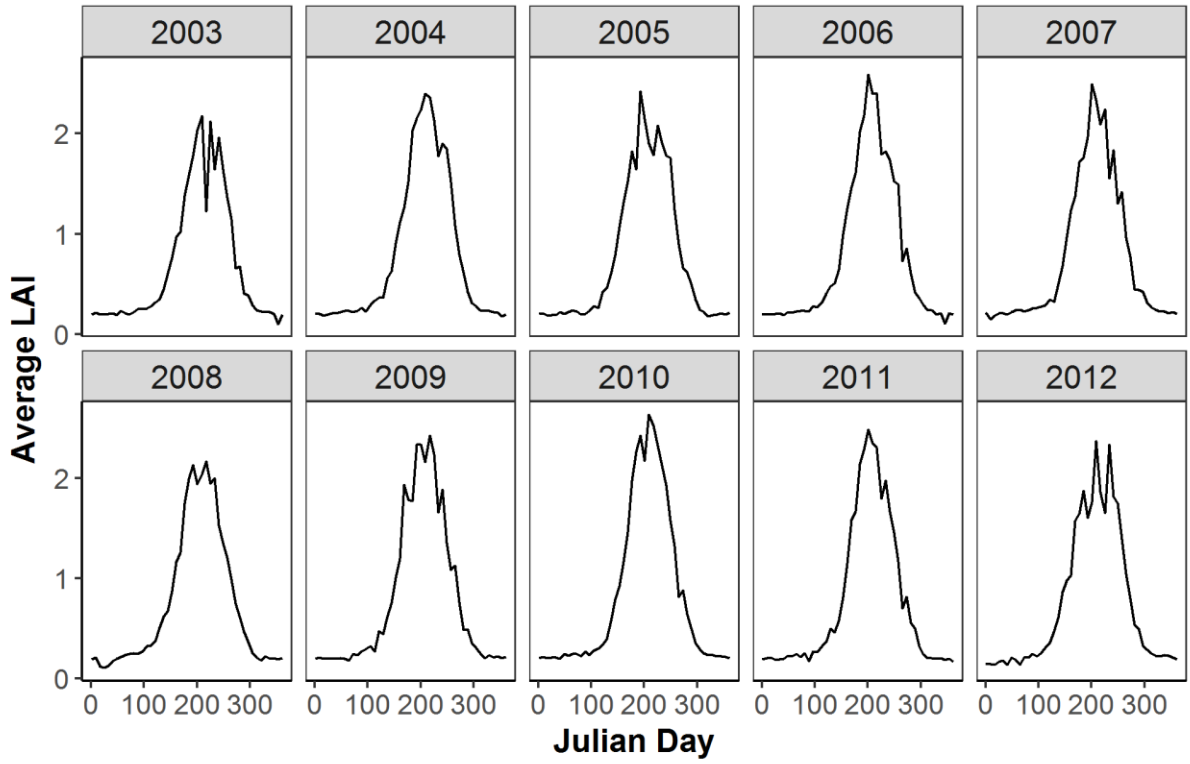

Fig. 7: Average MODIS LAI for each 8-days from 2003 to 2012 (QC=0)

To choose the appropriate change points for the growing season, change point detection is used as shown in Table 3. The change points are those with the maximum likelihood of minimizing the cost-penalty function. There are two obvious change points. The first occurs at the beginning of the spring season (growth dominated), where the LAI increases from a period of fixed initial background to a rapid increase. The second occurs at the beginning of winter season (senescence dominated) when the sharp deceleration of LAI tends to be the same as initial background LAI. These two change points indicate the start of the fast-growing period and the end of the rapid senescence period respectively. Based on the conservative principle, the minimum date of the first change point is chosen as the start day of the fast-growing season, and the maximum date of last change point is the end day of the senescence dominated period for the whole dataset.

Table 3: Detected change points of mean LAI (QC=0)

year	Change points (Julian Day)	Observation in the year

2003	137 169 185 209 217 241 265 281	18 22 24 27 28 31 34 36
2004	129 153 177 225 257 281	17 20 23 29 33 36
2005	129 153 185 201 249 265 289	17 20 24 26 32 34 37
2006	113 145 177 217 257 281	15 19 23 28 33 36
2007	129 145 169 193 225 257 273	17 19 22 25 29 33 35
2008	121 153 169 233 257 281	16 20 22 30 33 36
2009	113 145 161 185 225 241 273	15 19 21 24 29 31 35
2010	129 153 169 225 257 289	17 20 22 29 33 37
2011	145 161 177 217 257 289	19 21 23 28 33 37
2012	129 161 201 249 273	17 21 26 32 35
2013	137 153 169 193 225 249 281	18 20 22 25 29 32 36
2014	129 153 185 209 241 273	17 20 24 27 31 35
final choose	Start date{113}, end date{289}	Start date{15}, end date{37}

The start and end dates of the grass growth period are used to extract the modal value of the MODIS LAI (taken from those points with QC=0); this is the initial value of LAI (or background LAI) during the winter period (observation 1~14 and 37~46). The initial background LAI will be used in fitting our new growth function.

3.3. Estimated grazing-led LAI changes

The grazing-led LAI changes, calculated on a per pixel basis and plotted as maps, are shown in Fig. 8. Recall that LAI values are a measure of the leaf surface area per unit area and as such are dimensionless (m^2/m^2). They range from 0 to 15.34. Note that there is a consistent spatial pattern whereby the southeast part of the region has higher grazed LAI than that of its counterparts; this is similar to the pattern found by other researchers (Fan et al. 2010b). Given an estimate of the grazed LAIs, these figures can be converted to equivalent leaf mass and aggregated to a sum total for each year. This will be shown in the validation section of the results.

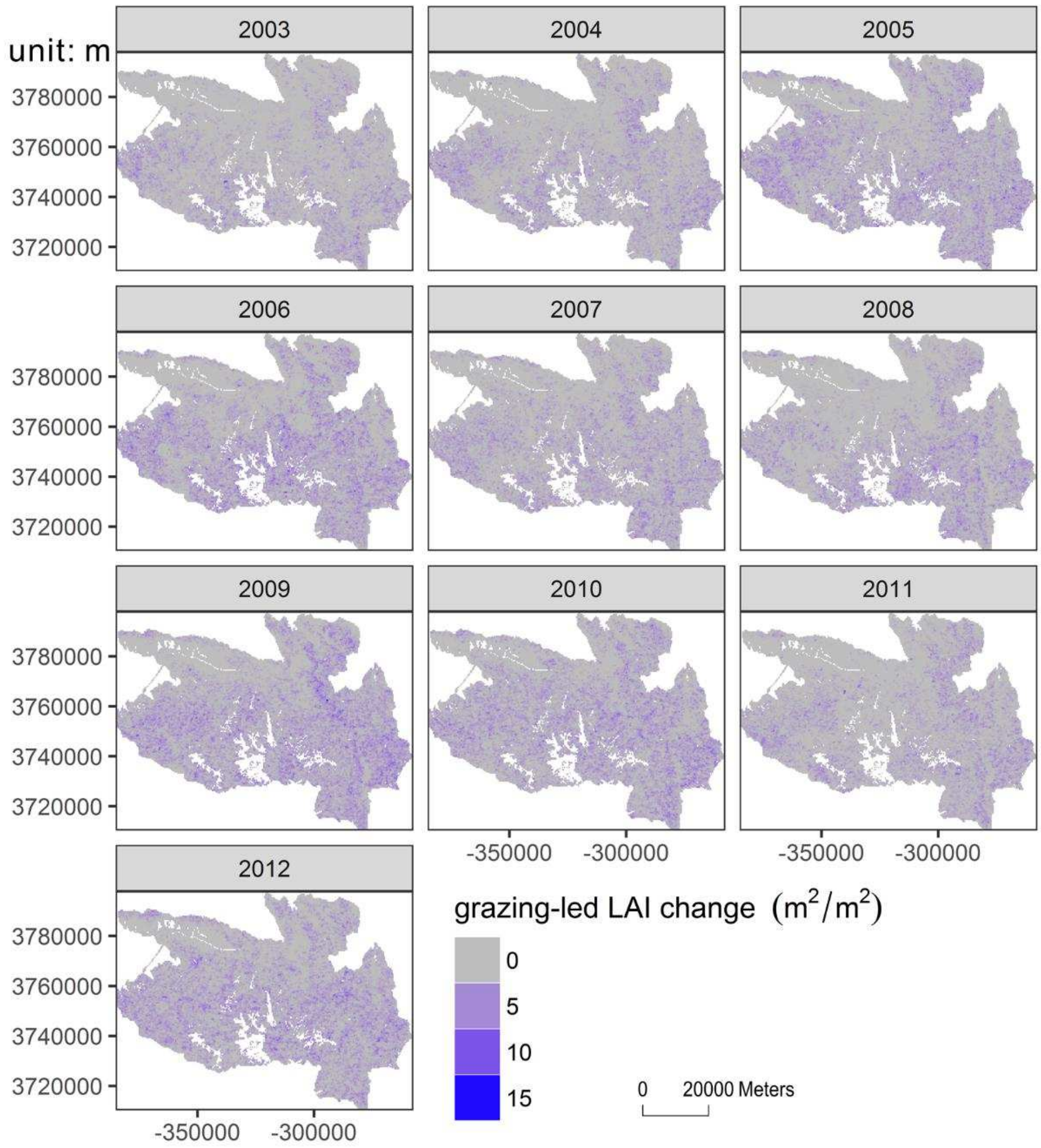

Fig. 8: Grazing-led LAI changes (without the effect of the previous grazing) of Zeku, 2003~2012

3.4. Modelling results vs MODIS NPP and in-situ measurements

The NPP was calculated on a daily basis for our improved LAI (Table 4, column "LUE-VPM NPP (improved LAI)"). In order to compare with the in situ observed data (Table 4, column "Converted in-situ NPP"), we aggregate the daily NPP from the first day of 2012 to the date listed in Table 4 (column: "collecting time", these are the date when the grass fresh weight were measured). The original MODIS NPP data are in Table 4 (column: "MODIS NPP"). In addition, with the purpose of showing our improved LAI performs better than the MODIS

LAI, we calculate the NPP using MODIS LAI as well (column: “LUE-VPM NPP (MODIS LAI)”).

Table 4: Validation with in-situ measured carbon mass (unit: gC/m^2)

ID	longtitute	latitute	altitute	collecting time	Converted in-situ NPP	LUE-VPM NPP (improved LAI)	MODIS NPP	LUE-VPM NPP (MODIS LAI)
1	101.13	35.31	3482	2012-08-06	143.56	191.47	151.12	182.79
2	101.08	35.27	3495	2012-08-05	548.06	285.35	203.60	264.61
3	101.32	35.27	3636	2012-08-06	180.38	245.00	175.12	223.42
4	101.73	35.06	3617	2012-08-07	335.81	316.31	194.16	272.44
5	101.80	35.06	3549	2012-08-08	233.40	235.56	167.36	228.64
6	100.87	35.22	3371	2012-08-09	193.42	NA	194.96	NA
7	100.87	35.22	3380	2012-08-09	346.88	NA	183.36	NA
8	101.01	35.19	3511	2012-08-06	290.71	301.43	219.12	269.31
9	101.46	35.04	3671	2012-08-08	103.15	256.47	156.64	202.58
10	100.91	35.39	3411	2012-08-07	149.98	245.32	170.16	230.09
11	100.94	35.39	3420	2012-08-07	288.73	271.83	170.24	243.14
12	101.15	35.30	3481	2012-08-06	139.91	230.29	146.64	194.44
13	101.18	35.29	3524	2012-08-06	321.60	254.39	161.76	210.04
14	101.70	35.03	3619	2012-08-10	328.38	339.67	188.80	262.48
15	101.61	35.08	3789	2012-08-07	346.54	295.67	195.84	289.53
mean					262.32	266.83	176.97	236.42

Since Root Mean Square Deviation (RMSE) can only report the difference between model results and validation observations, but not the significance level of these differences, we use Tukey's honest significance test (TukeyHSD test) (Tukey 1949) to report such a significance level (Table 5). It shows there is no significant difference between NPP calculated by LUE-VPM based on our improved LAI and converted in-situ measured carbon mass with a p-value equalling 0.998 (the RMSE between the two is 97.77 gC/m^2) Conversely the p-value between converted in-situ measured carbon mass and the MODIS NPP product is 0.011(the RMSE between the two is 133.98 gC/m^2), indicating the MODIS NPP product for Zeku is significantly different from the in-situ measured data. When keeping all the parameters of LUE-VPM the same, the p-value between converted in-situ measured NPP and the NPP calculated based on MODIS LAI is 0.760. In addition, from Table 4, the average converted NPP from in-situ measured data is 262.32 gC/m^2, while the NPP calculated by LUE-VPM based on our improved LAI is 266.83 gC/m^2, and if all the LUE-VPM parameters are kept the same, the average recalculated NPP by LUE-VPM based on MODIS LAI is 236.42 gC/m^2, which indicates that the improved LAI estimate has improved the accuracy of the NPP calculations on average.

Table 5: Multiple comparisons with one-way ANOVA test

(I) group	(J) group	Mean Difference (I-J)	Std. Error	Sig.	95% Confidence Interval	
					Lower Bound	Upper Bound
LUE-VPM NPP (improved LAI)	MODIS NPP	89.861*	26.350	.007	19.735	159.988
	Converted in-situ NPP	4.504	26.350	.998	-65.623	74.6301
	LUE-VPM NPP (MODIS LAI)	30.404	26.350	.658	-39.723	100.531
MODIS NPP	LUE-VPM NPP (improved LAI)	-89.862*	26.350	.007	-159.988	-19.735
	Converted in-situ NPP	-85.358*	26.350	.011	-155.485	-15.231
	LUE-VPM NPP (MODIS LAI)	-59.458	26.350	.123	-129.585	10.669
Converted in-situ NPP	LUE-VPM NPP (improved LAI)	-4.504	26.350	.998	-74.631	65.623
	MODIS NPP	85.358*	26.350	.011	15.231	155.485
	LUE-VPM NPP (MODIS LAI)	25.900	26.350	.760	-44.227	96.027
LUE-VPM NPP (MODIS LAI)	LUE-VPM NPP (improved LAI)	-30.404	26.350	.658	-100.537	39.723
	MODIS NPP	59.458	26.350	.123	-10.669	129.585
	Converted in-situ NPP	-25.900	26.350	.760	-96.027	44.227

*. The mean difference is significant at the 0.05 level.

Notes: Converted in-situ NPP is the converted NPP from in-situ measurement of grass fresh weight;
MODIS NPP is MOD17A3H (MODIS collection 6 NPP), which is public free from https://lpdaac.usgs.gov/dataset_discovery/modis/modis_products_table/mod17a3h_v006;
LUE-VPD (improved LAI) is the NPP calculated by Light Use Efficiency with Vegetation Photosynthesis Model based on improved LAI produced by this paper;
LUE-VPD (MODIS LAI) is the NPP calculated by Light Use Efficiency with Vegetation Photosynthesis Model based on MODIS LAI (MOD15A2H006, MODIS collection 6 LAI, which is public free from https://lpdaac.usgs.gov/dataset_discovery/modis/modis_products_table/mod15a2h_v006).

3.5. Carbon mass changes vs statistical livestock consumption

The following table (Table 6) shows the Pearson correlation matrix between the yearly aggregated grazed leaf mass based on LAI and the carbon mass calculated from raised livestock according to the statistics yearbook. The unit for carbon is 1×10^6 kgC. Herders do not sell yaks until there is insufficient feed from the grassland in Zeku to maintain the herd. They see yak as part of their property in the local culture. Hence there is there is no correlation (a Pearson correlation coefficient of -0.01) between raised yaks and estimated grazed carbon mass. However, sheep more accurately reflect the change in grassland provision and can be traded at any time and during any growth period as needed (correlation coefficient is 0.59). The overall correlation between sheep units of actual sheep and estimated grazed leaf mass is 0.42, while the p-value of a paired T-test is 0.71 (with R-squared= 0.17). This indicates a consistent trend between the estimated grazed amount of leaf mass and the associated consumed carbon mass over time.

Table 6: Pearson correlation matrix among raised livestock and identified grazed leaf mass

Pearson correlation	year	yak	horse	goat	sheep	total	leaf mass
year	1.00						
yak	-0.78	1.00					
horse	0.82	-0.61	1.00				
goat	-0.38	0.75	-0.49	1.00			
sheep	0.57	-0.68	0.32	-0.39	1.00		
total	-0.50	0.84	-0.36	0.71	-0.22	1.00	
leaf mass	0.28	-0.01	0.06	0.12	0.59	0.42	1.00

3.6. Impact of neighbour radius on the estimation of grazing-led LAI change

The temporal neighbourhood radius considered in the above estimation methodology could potentially have a significant effect on the estimation of grazing-led LAI change. There is a contradiction when choosing a proper neighbourhood radius. A smaller radius is expected to be more precise, but may equally underestimate grazing-led LAI change. A greater neighbour radius value would increase the error of the searching algorithm, especial near inflection points of the LAI growth curve. This section, therefore, explores this sensitivity. When setting the neighbour radius at values of 1, 2, 3 and 4 neighbouring points separately, the distributions of the aggregated grazing-led LAI changes for all of the pixels are shown in Fig. 9. It is clear that there are differences in the distributions between search radius 1 and search radius 2, and, likewise, 2 and 3. But values are almost the same between searching radius 3 and 4. Making a 'natural breaks' assumption, therefore, the optimal search radius value is 3 for the majority of the pixels in this sensitivity analysis. This can be further validated by plotting the histogram of the actual optimal neighbourhood radius used for each pixel (Fig. 10), of which the average optimal neighbourhood radius is 3.

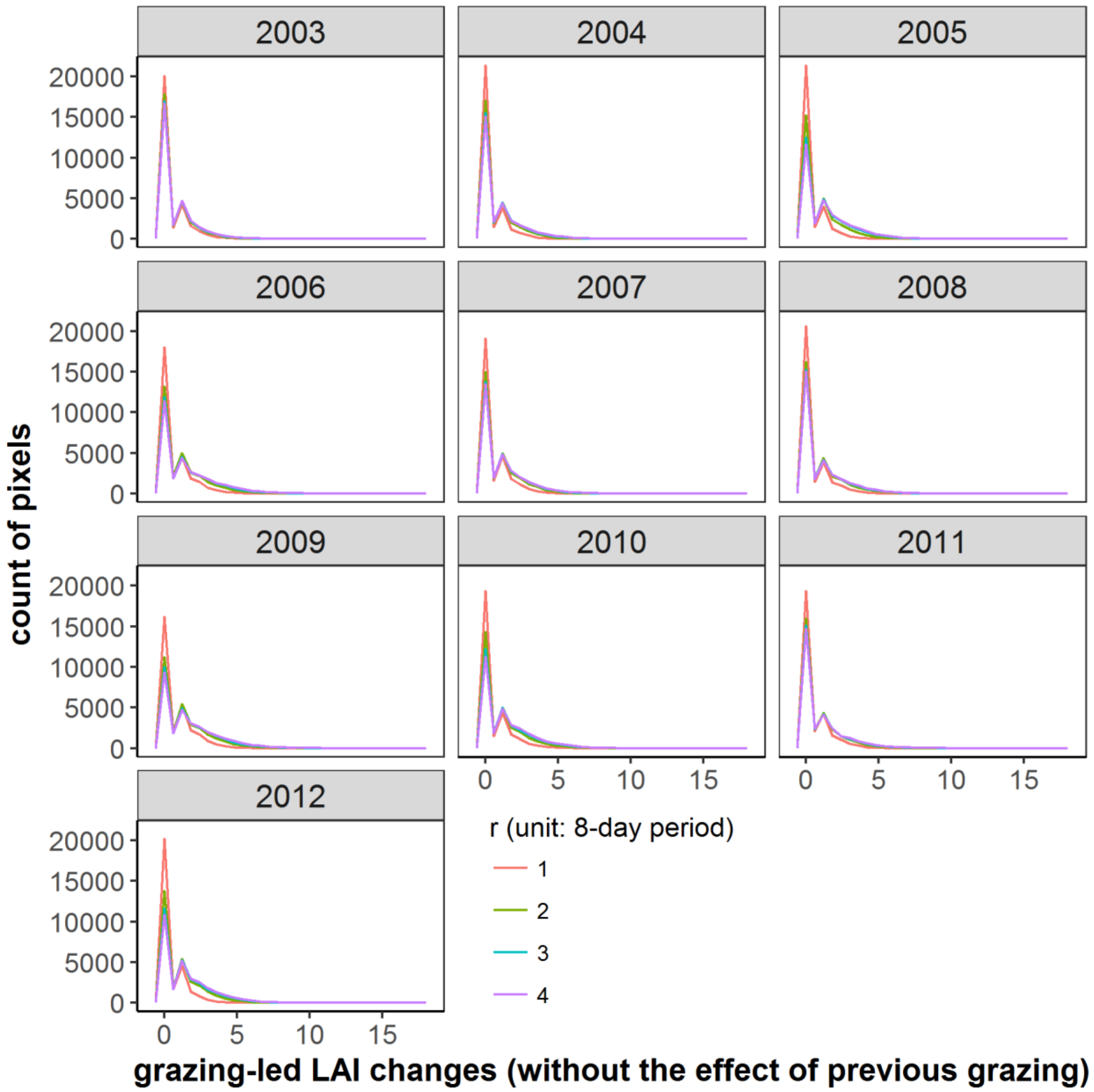

Fig. 9: distribution of estimated grazing-led LAI changes at neighbour radius 1, 2, 3 and 4

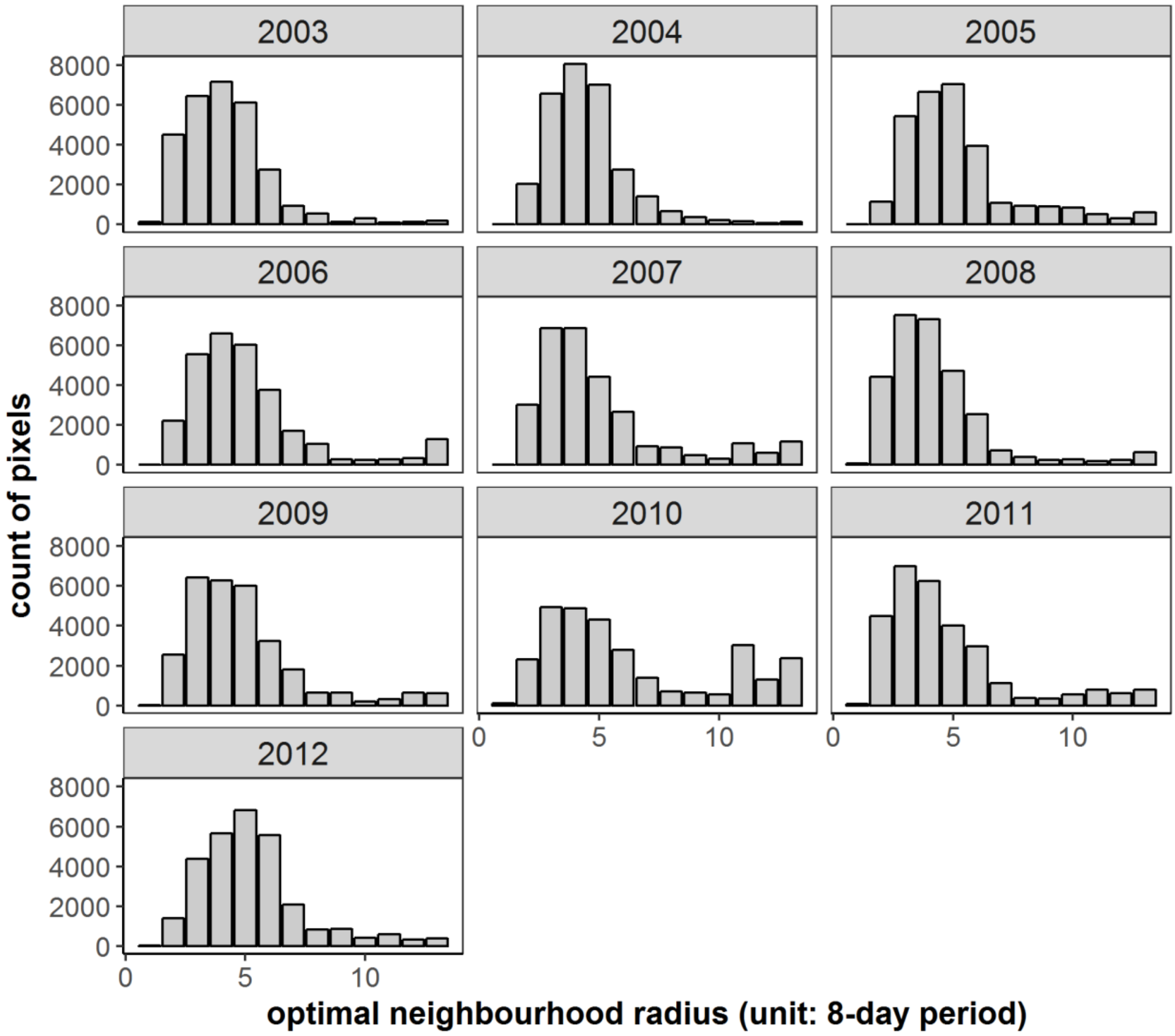

Fig. 10: Histogram of optimal neighbourhood radius for all pixels when choosing minimum fitting residuals.

3.7. Uncertainty of MODIS "good quality" LAI data

For each pixel, MODIS LAI estimations were associated with the day when the highest fPAR value was observed during every 8-day period, and the fPAR was estimated based on daily surface reflectance data (Knyazikhin et al. 1999). Unfortunately, this date has not been recorded in the MODIS LAI dataset. In Section 3.4, the time difference was used to as a weight and it was assumed that the observation date of the LAI value is exactly the same as MODIS LAI recorded date (Julian day 1, 9…361 of the year). This assumption would affect the weight in calculating grazing-led LAI changes. We, therefore, set up an uncertainty simulator, with the purpose of assessing the effect of the uncertainty of date in MODIS LAI on the time weight. Taking assumed weight ($\frac{i-m}{n-m}$ in Section 3.4) for example, we assume r, i, m, n can be any day during the 8-day period in reality, the values of which are then the random between 0 and 1 (within 1 unit of 8-day period). We use 10000 iterations to recalculate the possible actual weight (possible MODIS weight) and the mean and variance are plotted with regards to the different neighbourhood radius (Fig. 11). The result show that, on the average, the uncertainty of the date in the MODIS LAI data has a limited effect on the assumed weight. The variation of the weight in both assumed random date and simulated random date has the same range, and is mainly caused by the position of left or right neighbourhood point (in 8-day period unit) within the optimal neighbourhood radius. The most obvious difference during 8-day period in Fig. 12 is when the optimal neighbourhood radius equals 1, but as the average optimal neighbourhood radius is 3 (Figure 10), and more than 99.5% of the optimal neighbourhood radius is bigger than 1, this has a very limited effect on the estimation of grazing-led LAI changes.

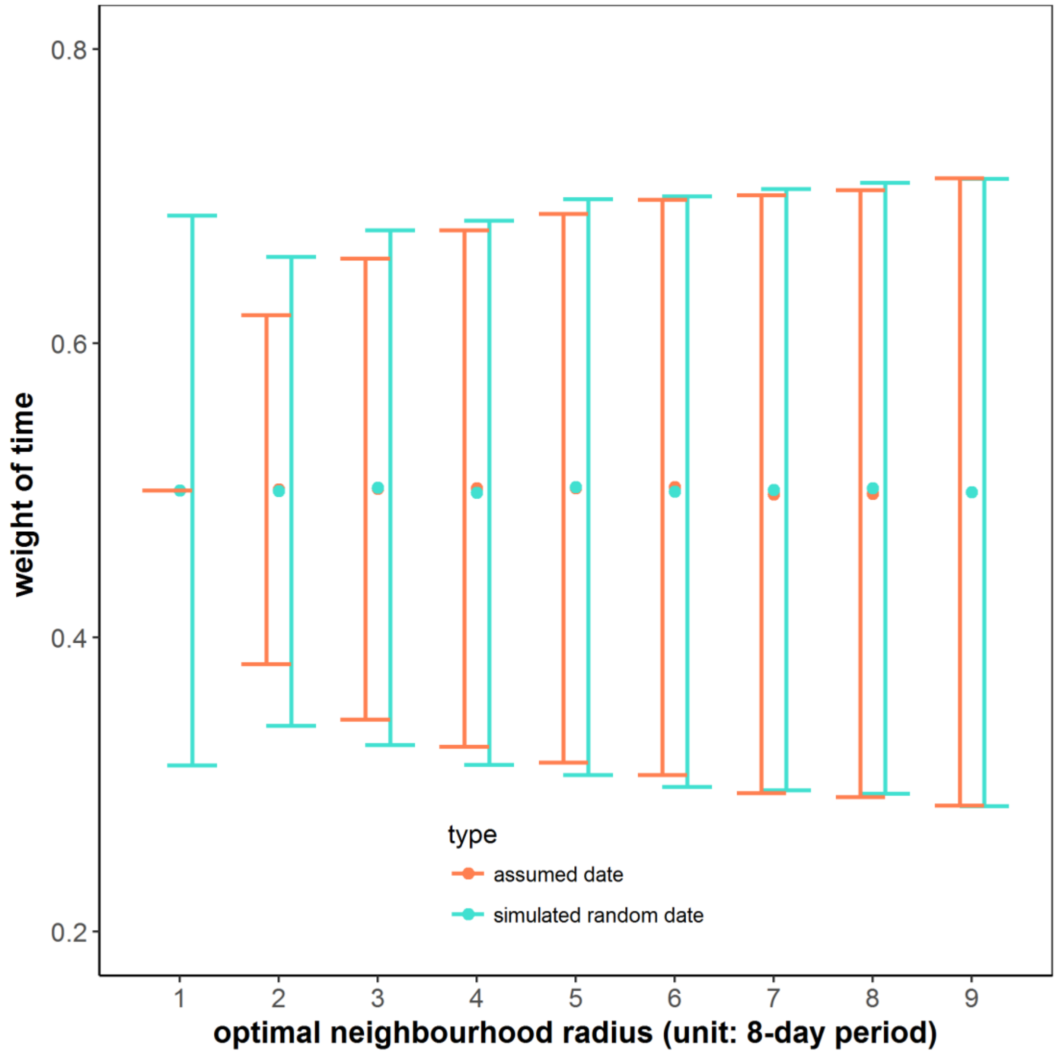

Fig. 11: Uncertainty of the date recorded in MODIS LAI on the weight of the estimation of grazing-led LAI changes

In term of the uncertainty of the value of MODIS “good quality” LAI, we use this percentage to filter out small LAI fluctuations, which may cause overestimation of the grazed LAI due to the effect of modelling error here, and background noise within the MODIS LAI data (Li et al. 2014). The effect of this uncertainty is therefore largely reduced during the estimation of grazing-led LAI changes.

5. Discussion

This paper developed a new growth grazing function with an estimation algorithm to identify the grazing-led LAI changes for each land pixel. It can extend the ability to extract large scale and real-time grazing information based on remote sensing data. The results were validated in two indirect validation ways. However, there are some aspects that could possibly affect the estimation accuracy of grazing-led LAI changes.

There is an assumption in Fig. 6 that the parameters k1 and k2 (growth and senescence coefficient) stay the same in spite of grazing, which may be not true in reality – plants may grow at different rates under grazing due to the over/under compensation of grazing both in the long term (McNaughton 1983) and short-term (Gignoux et al. 2001) grass development. In fact, a fitted growth function can only reflect growth parameters under the current grazing method and intensity. The local maximum LAI might be the result of either over- or under-compensation of grazing on the grass. If it is under compensated, the local maximum LAI is actually greater than the LAI of un-grazed and vice versa. But unfortunately, we don't know the actual LAI value if no grazing happens. It would require ground comparison experiments with remote sensing observations for all the pixels, which is an important research area but it is beyond the scope of this paper. Remote sensing can capture the status of grass under grazing, but cannot distinguish the kind of effect (over or under compensation) that is influencing grass growth, which is highly depended on grazing intensities (Hickman and Hartnett 2002). The figures here are an illustration of how grazing severity would affect the observed LAI and it's instantaneous growth rate if these parameters remain unchanged. This is why we cannot use this function to predict LAI under grazing. It is a year-round grass growth under grazing function rather than a predictive plant-livestock interaction function.

Grazing methods can affect the estimation of grazing-led LAI changes. Rotational grazing (or intermittent grazing), continuous grazing and un-grazed are the three common grazing methods on grassland in Zeku (Zhou et al. 2007). The grass on the un-grazed lands will be used as livestock winter forage; no grazing activities occur on these lands during the pasture growth period, so the LAI curve observed should be more close to a bell-shaped curve (Fig. 4) compared with that of the other two grazing methods. The difference between rotational and continuous grazing methods is that there are some “rest periods” for the grass on rotational grazing lands. They would present a fluctuated profile (see Fig. 5 for example). We can see in Fig. 6 that the mean LAI of 50% intermittent grazed (rotational grazing) is bigger than that of 50% continuous grazed (top right figure in Fig. 6). This is because the grazing intensity of the later (reduce 50% of the LAI continuously) is about two times than that of the former (reduce 50% of the LAI intermittently, it is approximately equivalent to 25% of the LAI reduction continuously); therefore, the mean value of LAI under 50% intermittent grazed land would be approximately equal to that of 25% continuous grazed (top left figure in Fig. 6). This theoretical result reveals the same outcomes at that of the field based comparison experiment reported by McMeekan and Walshe (1963) and Pavlů et al. (2003), that the stocking rate is the main factor affecting the growth of grass rather than grazing methods.

In the fast-growing period, the LAI value may be smaller than expected due to the grazing-led LAI changes (Garay et al. 1999; Sala et al. 1986). By utilising such features we can estimate the grazing-led LAI changes and the effect of the previous grazing. However, there would be an underestimation for continuous grazing as the MODIS LAI can only capture one fluctuation on the curve when livestock first start grazing. Again, the data on ground comparison experiments and grazing method for each land patch would need to be collected to deal with such underestimation. This would be extremely resource intensive, requiring long-term observations for future work.

In addition, some grass is harvested for winter forage, but the amount is very small and the local herders tend to keep one spare grassland patch un-grazed for winter (according to the field survey in 2012), which means that mowing activities have a little effect on the final estimation. For the non-growth periods, no matter how much grass had been consumed by livestock during winter, the grass will recover in the following year as long as the soil conditions and grassroots had not been severely affected by livestock browsing or trampling (Vallentine 2000). Further research on livestock browsing behaviours and the soil response to livestock grazing using remote sensing is the next challenge.

6. Conclusions

Large-scale monitoring of the grazing-led LAI changes based on MODIS LAI is possible when some characteristics of the grazing (such as the percentage of winter pasture used here), are known. Others factors such as time and duration of grazing, winter/summer pasture distribution, grazing methods, stocking rates, etc., could also potentially be used. This research is important for grazing management as it identifies the spatial pattern of grazing, which provides a useful proxy for managing the heterogeneity of grass forage distribution. In terms of methods, current reprocessing methods for MODIS LAI datasets are focused on producing smoother and more spatiotemporally consistent products by taking a spatial, temporal, or hybrid combination of weighted LAI. However, for grazing grasslands, the spatiotemporal weighted average LAI reprocessing methods diminish grazing information. In fact, for grassland vegetation, the temporal consistency is more dominant than the spatial consistency: every pixel is likely to have different conditions and/or different grazing patterns. We considered the characteristics of grassland growth, developed a new exponential growth function under grazing to produce the final improved LAI data (after grazing or if grazing happens) and expected LAI data (before grazing or if no grazing happens), which is suitable for extracting grazing information effectively and consistently. It provides a useful tool for the large-scale grazing monitoring and further assessment of the grassland ecosystem.

Acknowledgment

This work was partially funded by the National Key Research and Development Program of China (Grant no. 2016CYFA0602502) and the Chinese Scholarship Council. We thank Livestock Husbandry Bureau and Statistic Bureau of Zeku for providing in-situ grassland monitoring data and livestock statistical data. In addition, MODIS science team have provided excellent and accessible data products that made this paper possible. MODIS data were obtained from the Land Processes Distributed Active Archive Center (https://lpdaac.usgs.gov/).

Asam, S., Klein, D., & Dech, S. (2015). Estimation of grassland use intensities based on high spatial resolution LAI time series. Int. Arch. Photogramm. Remote Sens. Spatial Inf. Sci., XL-7/W3, 285-291

Baret, F., Hagolle, O., Geiger, B., Bicheron, P., Miras, B., Huc, M., Berthelot, B., Niño, F., Weiss, M., & Samain, O. (2007). LAI, fAPAR and fCover CYCLOPES global products derived from VEGETATION: Part 1: Principles of the algorithm. Remote Sensing of Environment, 110, 275-286

Bobée, C., Ottlé, C., Maignan, F., de Noblet-Ducoudré, N., Maugis, P., Lézine, A.M., & Ndiaye, M. (2012a). Analysis of vegetation seasonality in Sahelian environments using MODIS LAI, in association with land cover and rainfall. Journal of Arid Environments, 84, 38-50

Bobée, C., Ottlé, C., Maignan, F., de Noblet-Ducoudré, N., Maugis, P., Lézine, A.M., & Ndiaye, M. (2012b). Analysis of vegetation seasonality in Sahelian environments using MODIS LAI, in association with land cover and rainfall. Journal of Arid Environments, 84, 38-50

Borrás, L., Maddonni, G.A., & Otegui, M.E. (2003). Leaf senescence in maize hybrids: plant population, row spacing and kernel set effects. Field Crops Research, 82, 13-26

Buermann, W., Dong, J., Zeng, X., Myneni, R.B., & Dickinson, R.E. (2001). Evaluation of the utility of satellite-based vegetation leaf area index data for climate simulations. Journal of climate, 14, 3536-3550

Chen, J., Chen, J., Liao, A., Cao, X., Chen, L., Chen, X., He, C., Han, G., Peng, S., Lu, M., Zhang, W., Tong, X., & Mills, J. (2015). Global land cover mapping at 30 m resolution: A POK-based operational approach. ISPRS Journal of Photogrammetry and Remote Sensing, 103, 7-27

Chen, J.M., & Black, T. (1992). Defining leaf area index for non‐flat leaves. Plant, Cell & Environment, 15, 421-429

Chen, J.M., & Leblanc, S.G. (1997). A four-scale bidirectional reflectance model based on canopy architecture. IEEE Transactions on Geoscience and remote sensing, 35, 1316-1337

Croft, H., Chen, J.M., & Zhang, Y. (2014). The applicability of empirical vegetation indices for determining leaf chlorophyll content over different leaf and canopy structures. ecological complexity, 17, 119-130

De Kauwe, M.G., Disney, M.I., Quaife, T., Lewis, P., & Williams, M. (2011). An assessment of the MODIS collection 5 leaf area index product for a region of mixed coniferous forest. Remote Sensing of Environment, 115, 767-780

Dean, W.R.J., Hoffinan, M.T., Meadows, M.E., & Milton, S.J. (1995). Desertification in the semi-arid Karoo, South Africa: review and reassessment. Journal of Arid Environments, 30, 247-264

Deng, F., Chen, J., Plummer, S., Chen, M., & Pisek, J. (2006). Global LAI algorithm integrating the bidirectional information. IEEE Transactions on Geoscience and remote sensing, 44, 2219-2229

Fan, J.-W., Shao, Q.-Q., Liu, J.-Y., Wang, J.-B., Harris, W., Chen, Z.-Q., Zhong, H.-P., Xu, X.-L., & Liu, R.-G. (2010a). Assessment of effects of climate change and grazing activity on grassland yield in the Three Rivers Headwaters Region of Qinghai-Tibet Plateau, China. Environmental monitoring and assessment, 170, 571-584

Fan, J.-W., Shao, Q.-Q., Liu, J.-Y., Wang, J.-B., Harris, W., Chen, Z.-Q., Zhong, H.-P., Xu, X.-L., & Liu, R.-G. (2010b). Assessment of effects of climate change and grazing activity on grassland yield in the Three Rivers Headwaters Region of Qinghai–Tibet Plateau, China. Environmental monitoring and assessment, 170, 571-584

Fang, H., Liang, S., Townshend, J.R., & Dickinson, R.E. (2008). Spatially and temporally continuous LAI data sets based on an integrated filtering method: Examples from North America. Remote Sensing of Environment, 112, 75-93

Fang, S., Yu, W., & Qi, Y. (2015). Spectra and vegetation index variations in moss soil crust in different seasons, and in wet and dry conditions. International Journal of Applied Earth Observation and Geoinformation, 38, 261-266

Field, C.B., Randerson, J.T., & Malmström, C.M. (1995). Global net primary production: Combining ecology and remote sensing. Remote Sensing of Environment, 51, 74-88

Fu, P., & Rich, P.M. (2002). A geometric solar radiation model with applications in agriculture and forestry. Computers and Electronics in Agriculture, 37, 25-35

Galvão, L.S., Breunig, F.M., Santos, J.R.d., & Moura, Y.M.d. (2013). View-illumination effects on hyperspectral vegetation indices in the Amazonian tropical forest. International Journal of Applied Earth Observation and Geoinformation, 21, 291-300

Gao, Q., Qin, X., Wang, B., Guo, Y., Li, Y., Wan, Y., Jiangcun, W., & Ganjurjav (2013). Effects of topography and human activity on the net primary productivity (NPP) of alpine grassland in northern Tibet from 1981 to 2004. International Journal of Remote Sensing, 34, 2057-2069

Garay, A.H., Matthew, & Hodgson (1999). Tiller size/density compensation in perennial ryegrass miniature swards subject to differing defoliation heights and a proposed productivity index. Grass and Forage Science, 54, 347-356

Garrigues, S., Lacaze, R., Baret, F., Morisette, J.T., Weiss, M., Nickeson, J.E., Fernandes, R., Plummer, S., Shabanov, N.V., Myneni, R.B., Knyazikhin, Y., & Yang, W. (2008). Validation and intercomparison of global Leaf Area Index products derived from remote sensing data. Journal of Geophysical Research: Biogeosciences, 113, n/a-n/a

Gignoux, J., Fritz, H., Abbadie, L., & Loreau, M. (2001). Which Functional Processes Control the Short-Term Effect of Grazing on Net Primary Production in Grasslands? Oecologia, 129, 114-124

Hansen, M.C., DeFries, R.S., Townshend, J.R., Carroll, M., Dimiceli, C., & Sohlberg, R.A. (2003). The MODIS 500 meter global vegetation continuous field products. In, Second international workshop on the analysis of multitemporal remote sensing images, Ispra, Italy

Harris, R.B. (2010). Rangeland degradation on the Qinghai-Tibetan plateau: A review of the evidence of its magnitude and causes. Journal of Arid Environments, 74, 1-12

Harrison, M.T., Evans, J.R., & Moore, A.D. (2012). Using a mathematical framework to examine physiological changes in winter wheat after livestock grazing: 1. Model derivation and coefficient calibration. Field Crops Research, 136, 116-126

He, J., & Yang, K. (2011). China Meteorological Forcing Dataset. Cold and Arid Regions Science Data Center at Lanzhou

Hickman, K.R., & Hartnett, D.C. (2002). Effects of grazing intensity on growth, reproduction, and abundance of three palatable forbs in Kansas tallgrass prairie. Plant Ecology, 159, 23-33

Hill, M.J., Senarath, U., Lee, A., Zeppel, M., Nightingale, J.M., Williams, R.J., & McVicar, T.R. (2006). Assessment of the MODIS LAI product for Australian ecosystems. Remote Sensing of Environment, 101, 495-518

Hoffmann, W.A., da Silva, E.R., Machado, G.C., Bucci, S.J., Scholz, F.G., Goldstein, G., & Meinzer, F.C. (2005). Seasonal leaf dynamics across a tree density gradient in a Brazilian savanna. Oecologia, 145, 306-315

Horváth, L. (1993). The maximum likelihood method for testing changes in the parameters of normal observations. The Annals of statistics, 671-680

Huang, W., Bruemmer, B., & Huntsinger, L. (2016). Incorporating measures of grassland productivity into efficiency estimates for livestock grazing on the Qinghai-Tibetan Plateau in China. Ecological Economics, 122, 1-11

Huang, W., Bruemmer, B., & Huntsinger, L. (2017). Technical efficiency and the impact of grassland use right leasing on livestock grazing on the Qinghai-Tibetan Plateau. Land Use Policy, 64, 342-352

Jackson, B., Scargle, J.D., Barnes, D., Arabhi, S., Alt, A., Gioumousis, P., Gwin, E., Sangtrakulcharoen, P., Tan, L., & Tsai, T.T. (2005). An algorithm for optimal partitioning of data on an interval. IEEE Signal Processing Letters, 12, 105-108

Jensen, J.L.R., Humes, K.S., Hudak, A.T., Vierling, L.A., & Delmelle, E. (2011). Evaluation of the MODIS LAI product using independent lidar-derived LAI: A case study in mixed conifer forest. Remote Sensing of Environment, 115, 3625-3639

Jin, H., Li, A., Bian, J., Nan, X., Zhao, W., Zhang, Z., & Yin, G. (2017). Intercomparison and validation of MODIS and GLASS leaf area index (LAI) products over mountain areas: A case study in southwestern China. International Journal of Applied Earth Observation and Geoinformation, 55, 52-67

Johnson, I., & Thornley, J. (1983). Vegetative crop growth model incorporating leaf area expansion and senescence, and applied to grass. Plant, Cell & Environment, 6, 721-729

Johnson, I.R., Thornley, J.H., Frantz, J.M., & Bugbee, B. (2010). A model of canopy photosynthesis incorporating protein distribution through the canopy and its acclimation to light, temperature and CO2. Annals of Botany, 106, 735-749

Jonckheere, I., Fleck, S., Nackaerts, K., Muys, B., Coppin, P., Weiss, M., & Baret, F. (2004). Review of methods for in situ leaf area index determination: Part I. Theories, sensors and hemispherical photography. Agricultural and Forest Meteorology, 121, 19-35

Killick, R., & Eckley, I. (2014). changepoint: An R package for changepoint analysis. Journal of Statistical Software, 58, 1-19

Killick, R., Fearnhead, P., & Eckley, I.A. (2012). Optimal detection of changepoints with a linear computational cost. Journal of the American Statistical Association, 107, 1590-1598

Knyazikhin, Y., Glassy, J., Privette, J., Tian, Y., Lotsch, A., Zhang, Y., Wang, Y., Morisette, J., Votava, P., & Myneni, R. (1999). MODIS leaf area index (LAI) and fraction of photosynthetically active radiation absorbed by vegetation (FPAR) product (MOD15) algorithm theoretical basis document. Theoretical Basis Document, NASA Goddard Space Flight Center, Greenbelt, MD, 20771

Knyazikhin, Y., Martonchik, J., Myneni, R.B., Diner, D., & Running, S.W. (1998a). Synergistic algorithm for estimating vegetation canopy leaf area index and fraction of absorbed photosynthetically active radiation from MODIS and MISR data. Journal of Geophysical Research: Atmospheres, 103, 32257-32275

Knyazikhin, Y., Martonchik, J.V., Myneni, R.B., Diner, D.J., & Running, S.W. (1998b). Synergistic algorithm for estimating vegetation canopy leaf area index and fraction of absorbed photosynthetically active radiation from MODIS and MISR data. Journal of Geophysical Research: Atmospheres, 103, 32257-32275

Lai, Q., Li, Q.-f., Morigen, A., Shi, G.-h., & Wu, X.-b. (2008). A Study on Factors Affecting Moisture Content Measurement and Ratio of Forage Fresh Weight to Dry Weight [J]. Chinese Journal of Grassland, 4, 016

Lebert, T., Benjaminsen, T., Sjaastad, E., Rohde, R., & Wisborg, P. (2006). Land Reform, Range Ecology, and Carrying Capacities in Namaqualand, South Africa. Annals of the Association of American Geographers, 96, 524-540

Leopold, A., Niedergang-Kamien, E., & Janick, J. (1959). Experimental Modification of Plant Senescence. Plant Physiology, 34, 570

Li, A., Bian, J., Lei, G., & Huang, C. (2012). Estimating the Maximal Light Use Efficiency for Different Vegetation through the CASA Model Combined with Time-Series Remote Sensing Data and Ground Measurements. Remote Sensing

Li, Z., Tang, H., Xin, X., Zhang, B., & Wang, D. (2014). Assessment of the MODIS LAI Product Using Ground Measurement Data and HJ-1A/1B Imagery in the Meadow Steppe of Hulunber, China. Remote Sensing, 6, 6242

Liu, R., Shang, R., Liu, Y., & Lu, X. (2017). Global evaluation of gap-filling approaches for seasonal NDVI with considering vegetation growth trajectory, protection of key point, noise resistance and curve stability. Remote Sensing of Environment, 189, 164-179

Los, S.O., North, P.R.J., Grey, W.M.F., & Barnsley, M.J. (2005). A method to convert AVHRR Normalized Difference Vegetation Index time series to a standard viewing and illumination geometry. Remote Sensing of Environment, 99, 400-411

Maselli, F., Argenti, G., Chiesi, M., Angeli, L., & Papale, D. (2013). Simulation of grassland productivity by the combination of ground and satellite data. Agriculture, ecosystems & environment, 165, 163-172

Matches, A.G. (1992). Plant response to grazing: a review. Journal of production agriculture, 5, 1-7

Mayr, M.J., & Samimi, C. (2015). Comparing the dry season in-situ Leaf Area Index (LAI) derived from high-resolution rapideye imagery with MODIS LAI in a namibian Savanna. Remote Sensing, 7, 4834-4857

McMeekan, C., & Walshe, M. (1963). The inter-relationships of grazing method and stocking rate in the efficiency of pasture utilization by dairy cattle. The Journal of Agricultural Science, 61, 147-166

McNaughton, S. (1983). Compensatory plant growth as a response to herbivory. Oikos, 329-336

Miller-Goodman, M., Moser, L.E., Waller, S.S., Brummer, J., & Reece, P. (1999). Canopy analysis as a technique to characterize defoliation intensity on Sandhills range. Journal of Range Management, 357-362

Monteith, J., & Reifsnyder, W.E. (1974). Principles of Environmental Physics. Physics Today, 27, 51

Myneni, R., & K., Y. (2015). MOD15A2H MODIS/Terra Leaf Area Index/FPAR 8-Day L4 Global 500m SIN Grid V006. NASA EOSDIS Land Processes DAAC

Myneni, R., Knyazikhin, Y., & Park, T. (2015). MOD15A2H MODIS/Terra Leaf Area Index/FPAR 8-Day L4 Global 500 m SIN Grid V006. NASA EOSDIS Land Processes DAAC. Available online: https://lpdaac. usgs. gov/dataset_discovery/modis/modis_products_table/mod15a2h_v006 (accessed on 16 October 2016)

NY/T635, C.N.C. (2002). Calculation of carrying capability of the natural grassland [S]. In

Nyima, Y. (2015). What factors determine carrying capacity? A case study from pastoral Tibet. Area, 47, 73-80

Palmer, A.R., & Bennett, J.E. (2013). Degradation of communal rangelands in South Africa: towards an improved understanding to inform policy. AFRICAN JOURNAL OF RANGE & FORAGE SCIENCE, 30, 57-63

Pavlů, V., Hejcman, M., Pavlů, L., & Gaisler, J. (2003). Effect of rotational and continuous grazing on vegetation of an upland grassland in the Jizerské hory Mts., Czech Republic. Folia Geobotanica, 38, 21-34

Piñeiro, G., Oesterheld, M., & Paruelo, J.M. (2006). Seasonal Variation in Aboveground Production and Radiation-Use Efficiency of Temperate Rangelands Estimated through Remote Sensing. Ecosystems, 9, 357-373

Potter, C.S., Randerson, J.T., Field, C.B., Matson, P.A., Vitousek, P.M., Mooney, H.A., & Klooster, S.A. (1993). Terrestrial ecosystem production: A process model based on global satellite and surface data. Global Biogeochemical Cycles, 7, 811-841

Prieto-Blanco, A., North, P.R.J., Barnsley, M.J., & Fox, N. (2009). Satellite-driven modelling of Net Primary Productivity (NPP): Theoretical analysis. Remote Sensing of Environment, 113, 137-147

Ruimy, A., Kergoat, L., & Bondeau, A. (1999). Comparing global models of terrestrial net primary productivity (NPP): Analysis of differences in light absorption and light-use efficiency. Global Change Biology, 5, 56-64

Running, S. (2015). User's Guide GPP and NPP (MOD17A2/A3) Products

Running, S.W., Thornton, P.E., Nemani, R., & Glassy, J.M. (2000). Global Terrestrial Gross and Net Primary Productivity from the Earth Observing System. In O.E. Sala, R.B. Jackson, H.A. Mooney, & R.W. Howarth (Eds.), Methods in ecosystem science (pp. 44-57). New York, NY: Springer New York

Running, S.W., & Zhao, M. (2015). Daily GPP and Annual NPP (MOD17A2/A3) Products NASA Earth Observing System MODIS Land Algorithm

Russell, G., Marshall, B., & Jarvis, P.G. (1990). Plant canopies: their growth, form and function. Cambridge University Press

Sala, O., Oesterheld, M., León, R., & Soriano, A. (1986). Grazing effects upon plant community structure in subhumid grasslands of Argentina. Plant Ecology, 67, 27-32

Savitzky, A., & Golay, M.J. (1964). Smoothing and differentiation of data by simplified least squares procedures. Analytical chemistry, 36, 1627-1639

Swain, C.K., Bhattacharyya, P., Singh, N.R., Neogi, S., Sahoo, R.K., Nayak, A.K., Zhang, G., & Leclerc, M.Y. (2016). Net ecosystem methane and carbon dioxide exchange in relation to heat and carbon balance in lowland tropical rice. Ecological Engineering, 95, 364-374

Thornley, J.H.M., & Johnson, I.R. (1990). Plant and crop modelling: a mathematical approach to plant and crop physiology. Oxford: Clarendon

Tian, Y., Dickinson, R., Zhou, L., Zeng, X., Dai, Y., Myneni, R., Knyazikhin, Y., Zhang, X., Friedl, M., & Yu, H. (2004). Comparison of seasonal and spatial variations of leaf area index and fraction of absorbed photosynthetically active radiation from Moderate Resolution Imaging Spectroradiometer (MODIS) and Common Land Model. Journal of Geophysical Research: Atmospheres, 109

Tsalyuk, M., Kelly, M., Koy, K., Getz, W.M., & Butterfield, H.S. (2015). Monitoring the Impact of Grazing on Rangeland Conservation Easements Using MODIS Vegetation Indices. Rangeland Ecology & Management, 68, 173-185

Tukey, J.W. (1949). Comparing individual means in the analysis of variance. Biometrics, 99-114

Vallentine, J.F. (2000). Grazing management. Elsevier

Verger, A., Baret, F., Weiss, M., Filella, I., & Peñuelas, J. (2015). GEOCLIM: A global climatology of LAI, FAPAR, and FCOVER from VEGETATION observations for 1999–2010. Remote Sensing of Environment, 166, 126-137

Verhoef, W. (1984). Light scattering by leaf layers with application to canopy reflectance modeling: the SAIL model. Remote Sensing of Environment, 16, 125-141

Vermote, E. (2015). MOD09A1 MODIS/Terra Surface Reflectance 8-Day L3 Global 500m SIN Grid V006. NASA EOSDIS Land Processes DAAC. https://doi.org/10.5067/modis/mod09a1.006

Verrelst, J., van der Tol, C., Magnani, F., Sabater, N., Rivera, J.P., Mohammed, G., & Moreno, J. (2016). Evaluating the predictive power of sun-induced chlorophyll fluorescence to estimate net photosynthesis of vegetation canopies: A SCOPE modeling study. Remote Sensing of Environment, 176, 139-151

Wang, Y., Woodcock, C.E., Buermann, W., Stenberg, P., Voipio, P., Smolander, H., Häme, T., Tian, Y., Hu, J., Knyazikhin, Y., & Myneni, R.B. (2004). Evaluation of the MODIS LAI algorithm at a coniferous forest site in Finland. Remote Sensing of Environment, 91, 114-127

Wei, S., Wang, X., Shi, D., Li, Y., Zhang, J., Liu, P., Zhao, B., & Dong, S. (2016). The mechanisms of low nitrogen induced weakened photosynthesis in summer maize (Zea mays L.) under field conditions. Plant Physiology and Biochemistry, 105, 118-128

Xiao, X., Zhang, Q., Braswell, B., Urbanski, S., Boles, S., Wofsy, S., Moore Iii, B., & Ojima, D. (2004). Modeling gross primary production of temperate deciduous broadleaf forest using satellite images and climate data. Remote Sensing of Environment, 91, 256-270

Xiao, Z., Liang, S., Wang, J., Jiang, B., & Li, X. (2011). Real-time retrieval of Leaf Area Index from MODIS time series data. Remote Sensing of Environment, 115, 97-106

Yang, W., Huang, D., Tan, B., Stroeve, J.C., Shabanov, N.V., Knyazikhin, Y., Nemani, R.R., & Myneni, R.B. (2006). Analysis of leaf area index and fraction of PAR absorbed by vegetation products from the terra MODIS sensor: 2000-2005. IEEE Transactions on Geoscience and remote sensing, 44, 1829-1842

Yuan, H., Dai, Y., Xiao, Z., Ji, D., & Shangguan, W. (2011). Reprocessing the MODIS Leaf Area Index products for land surface and climate modelling. Remote Sensing of Environment, 115, 1171-1187

Zhang, N.R., & Siegmund, D.O. (2007). A modified Bayes information criterion with applications to the analysis of comparative genomic hybridization data. Biometrics, 63, 22-32

Zhang, Y., Qu, Y., Wang, J., Liang, S., & Liu, Y. (2012). Estimating leaf area index from MODIS and surface meteorological data using a dynamic Bayesian network. Remote Sensing of Environment, 127, 30-43

Zhang, Y., Song, C., Band, L.E., Sun, G., & Li, J. (2017). Reanalysis of global terrestrial vegetation trends from MODIS products: Browning or greening? Remote Sensing of Environment, 191, 145-155

Zhang, Y., Zhao, W., He, J., & Zhang, K. (2016). Energy exchange and evapotranspiration over irrigated seed maize agroecosystems in a desert-oasis region, northwest China. Agricultural and Forest Meteorology, 223, 48-59

Zhou, H.-k., Wang, Q.-j., Zhao, L., Han, F., & Zhang, Y. (2007). The present situation of grassland and the strategies of sustainable development of animal husbandry in Zeku County, Qinghai Province [J]. Pratacultural Science, 3, 018

LIST OF FIGURE CAPTIONS

Fig. 1: Percentage of "good quality" (QC=0) pixels for MODIS LAI in Zeku, China

Fig. 2: Land Cover of Zeku, 2010

Fig. 3: Conceptual framework for quantifying grazing based on LAI data

Fig. 4: LAI during a regrowth follows a bell curve as the canopy develops from low LAI (Phase I: low LAI increase rate) to maximum LAI (Phase II: high increase rate, growth dominated) and then to low LAI again (Phase 3: high LAI decrease, senescence dominated).

Fig. 5: Estimation of grazing-led LAI changes estimation

Fig. 6: The effect of grazing severity on the observed LAI and instantaneous net growth rate of LAI, with for example: k1= 0.16, k2=0.0003, C=-14. c and d are $L_t{}'$

Fig. 7: Average MODIS LAI for each 8-days from 2003 to 2012 (QC=0)

Fig. 8: Grazing-led LAI changes (without the effect of previous grazing) of Zeku, 2003~2012

Fig. 9: distribution of estimated grazing-led LAI changes at neighbour radius 1, 2, 3 and 4

Fig. 10: Histogram of optimal neighbourhood radius for all pixels when choosing minimum fitting residuals.

Fig. 11: Uncertainty of the date recorded in MODIS LAI on the weight of the estimation of grazing-led LAI changes